REPORT DOCUMENTATION PAGE	Form Approved OMB No. 0704-0188

PLEASE DO NOT RETURN YOUR FORM TO THE ABOVE ADDRESS.

1. REPORT DATE *(DD-MM-YYYY)*	2. REPORT TYPE	3. DATES COVERED *(From - To)*
26-08-2007	Final Report	1-May-2001 - 31-Oct-2006

4. TITLE AND SUBTITLE

Modeling Plastic Shocks in Periodic Laminates with Gradient Plasticity Theories

5a. CONTRACT NUMBER

DAAD19-01-1-0568

5b. GRANT NUMBER

61102

5c. PROGRAM ELEMENT NUMBER

6. AUTHOR(S)

G. Ravichandran, A. Molinari

5d. PROJECT NUMBER

5e. TASK NUMBER

5f. WORK UNIT NUMBER

7. PERFORMING ORGANIZATION NAME(S) AND ADDRESS(ES)

California Institute of Technology
Sponsored Research MC 201-15
California Institute of Technology
Pasadena, CA 91125

8. PERFORMING ORGANIZATION REPORT NUMBER

9. SPONSORING/MONITORING AGENCY NAME(S) AND ADDRESS(ES)

U.S. Army Research Office
P.O. Box 12211
Research Triangle Park, NC 27709-2211

10. SPONSOR/MONITOR'S ACRONYM(S)

ARO

11. SPONSOR/MONITOR'S REPORT NUMBER(S)

41690-EG.1

12. DISTRIBUTION/AVAILABILITY STATEMENT

Approved for Public Release; Distribution Unlimited

13. SUPPLEMENTARY NOTES

The views, opinions and/or findings contained in this report are those of the author(s) and should not contrued as an official Department

14. ABSTRACT

Steady plastic shocks generated by planar impact on metal-polymer laminate composites, are analyzed in the framework of gradient plasticity theories. The laminate material has a periodic structure with unit cell composed of two layers of different materials. First and second order gradient plasticity theories are used to model the structure of steady plastic shocks. In both theories, the effect of the internal structure is accounted for at the macroscopic level by two material parameters depending upon the layer's thickness and the properties of constituents. Those two structure-parameters are shown to be uniquely determined from experimental data.

15. SUBJECT TERMS

Solid Mechanics; shock waves; heterogeneous materials; dispersion; gradient theories; scaling laws

16. SECURITY CLASSIFICATION OF:			17. LIMITATION OF ABSTRACT	18. NUMBER OF PAGES	19a. NAME OF RESPONSIBLE PERSON
a. REPORT	b. ABSTRACT	c. THIS PAGE			Guruswami Ravichandran
unclass	unclass	unclass	SAR	53	19b. TELEPHONE NUMBER *(Include area code)* 626-395-4525

Report Title

Modeling plastic shocks in periodic laminates with gradient plasticity theories

ABSTRACT

Steady plastic shocks generated by planar impact on metal-polymer laminate composites, are analyzed in the framework of gradient plasticity theories. The laminate material has a periodic structure with unit cell composed of two layers of different materials. First and second order gradient plasticity theories are used to model the structure of steady plastic shocks. In both theories, the effect of the internal structure is accounted for at the macroscopic level by two material parameters depending upon the layer's thickness and the properties of constituents. Those two structure-parameters are shown to be uniquely determined from experimental data. Theoretical predictions are compared with experiments for different cell sizes and for various shock intensities. In particular, the following experimental features are well reproduced by the modeling:

- the shock width is proportional to the cell size;
- the magnitude of strain rate is inversely proportional to cell size and increases with the amplitude of applied stress following a power law.

While these results are equally described by both the plasticity theories, the first gradient plasticity approach seems to be favored when comparing the structure of the shock front to experimental data.

List of papers submitted or published that acknowledge ARO support during this reporting period. List the papers, including journal references, in the following categories:

(a) Papers published in peer-reviewed journals (N/A for none)

Y. Gu and G. Ravichandran, "Prediction of incipient shear band trajectories in a thick wall cylinder explosion test," Experimental Mechanics, 45, 447-450 (2005)

Y. Gu and G. Ravichandran, "Prediction of incipient shear band trajectories in a thick wall cylinder explosion test," Experimental Mechanics, 45, 447-450 (2005)

Y. Gu and G. Ravichandran, "Dynamic behavior of selected ceramic powders," International Journal of Impact Engineering, 32, 1768-1785 (2006)

A. Molinari and G. Ravichandran, "Modeling plastic shocks in periodic laminates with gradient plasticity theories," Journal of the Mechanics and Physics of Solids, 54, 2495-2526 (2006)

Number of Papers published in peer-reviewed journals: 4.00

(b) Papers published in non-peer-reviewed journals or in conference proceedings (N/A for none)

Number of Papers published in non peer-reviewed journals: 0.00

(c) Presentations

Number of Presentations: 0.00

Non Peer-Reviewed Conference Proceeding publications (other than abstracts):

Y. Gu and G. Ravichandran., 'Shock Hugoniot Data for Selected Ceramic Powders', Proceeding of the Eleventh International Symposium on Plasticity and Its Current Applications, pp. 331-333, (2005).

Number of Non Peer-Reviewed Conference Proceeding publications (other than abstracts): 1

Peer-Reviewed Conference Proceeding publications (other than abstracts):

Number of Peer-Reviewed Conference Proceeding publications (other than abstracts): 0

(d) Manuscripts

Number of Manuscripts: 0.00

Number of Inventions:

Graduate Students

NAME	PERCENT_SUPPORTED
FTE Equivalent:	
Total Number:	

Names of Post Doctorates

NAME	PERCENT_SUPPORTED
Y. Gu	1.00
FTE Equivalent:	**1.00**
Total Number:	**1**

Names of Faculty Supported

NAME	PERCENT_SUPPORTED	National Academy Member
G. Ravichandran	0.05	No
FTE Equivalent:	**0.05**	
Total Number:	**1**	

Names of Under Graduate students supported

NAME	PERCENT_SUPPORTED
FTE Equivalent:	
Total Number:	

Student Metrics

This section only applies to graduating undergraduates supported by this agreement in this reporting period

The number of undergraduates funded by this agreement who graduated during this period:	0.00
The number of undergraduates funded by this agreement who graduated during this period with a degree in science, mathematics, engineering, or technology fields:.....	0.00
The number of undergraduates funded by your agreement who graduated during this period and will continue to pursue a graduate or Ph.D. degree in science, mathematics, engineering, or technology fields:.....	0.00
Number of graduating undergraduates who achieved a 3.5 GPA to 4.0 (4.0 max scale):	0.00
Number of graduating undergraduates funded by a DoD funded Center of Excellence grant for Education, Research and Engineering:	0.00
The number of undergraduates funded by your agreement who graduated during this period and intend to work for the Department of Defense	0.00
The number of undergraduates funded by your agreement who graduated during this period and will receive scholarships or fellowships for further studies in science, mathematics, engineering or technology fields:	0.00

Names of Personnel receiving masters degrees

NAME
Total Number:

Names of personnel receiving PHDs

NAME
Total Number:

Names of other research staff

NAME	PERCENT_SUPPORTED	
A. Molinari	0.05	No
FTE Equivalent:	**0.05**	
Total Number:	**1**	

Sub Contractors (DD882)

Inventions (DD882)

Modeling plastic shocks in periodic laminates with gradient plasticity theories

Alain Molinari[a] and Guruswami Ravichandran[b]

[a]Laboratoire de Physique et Mécanique des Matériaux
Université de Metz, Ile du Saulcy, 57045 Metz Cedex 01, France
[b]Graduate Aeronautical Laboratories
California Institute of Technology, Pasadena, California 91125, USA

Abstract:

Steady plastic shocks generated by planar impact on metal-polymer laminate composites, are analyzed in the framework of gradient plasticity theories. The laminate material has a periodic structure with unit cell composed of two layers of different materials. First and second order gradient plasticity theories are used to model the structure of steady plastic shocks. In both theories, the effect of the internal structure is accounted for at the macroscopic level by two material parameters depending upon the layer's thickness and the properties of constituents. Those two structure-parameters are shown to be uniquely determined from experimental data. Theoretical predictions are compared with experiments for different cell sizes and for various shock intensities. In particular, the following experimental features are well reproduced by the modeling:

- the shock width is proportional to the cell size;
- the magnitude of strain rate is inversely proportional to cell size and increases with the amplitude of applied stress following a power law.

While these results are equally described by both the plasticity theories, the first gradient plasticity approach seems to be favored when comparing the structure of the shock front to experimental data.

1) **Introduction**

The visco-plastic response of metals and polymers at high loading rates can be investigated using shock wave experiments. Plate impact experiments have provided a large quantity of experimental data on steady plastic shocks, especially for polycrystalline metals, Rice et al (1958), Johnson and Barker (1969), Swegle and Grady (1985). By analyzing a stationary plastic shock, the following data can be obtained: (i) stress amplitude, (ii) particle velocity versus time at a given point, (iii) plastic-shock velocity C, (iv) particle velocity v^- behind the shock front and (v) maximum strain rate within the shock front layer. The Hugoniot curve is an important material characteristic obtained from shock analysis. From data (iii) and (iv), a linear relationship between C and v^- is obtained from which the Hugoniot can be deduced (see for example, Molinari and Ravichandran (2004)).

The problem of relating shock experimental data to material properties is a problem of fundamental importance which was studied in detail for certain classes of materials; see for example, Clifton (1971), Swegle and Grady (1985), Molinari and Ravichandran (2004). The shock front is a thin layer where particle velocity, stress and strain sustain a rapid variation. The spatial distribution of those quantities within the shock front, which is usually referred to as the shock structure, is in many cases controlled by viscous effects. For polycrystalline metals, viscous effects can be related to dislocation gliding. For more details and references, it is referred to Molinari and Ravichandran (2004), where a detailed analysis is given for moderate shocks in metals, with a specific application to aluminum. As mentioned before, the maximum of the strain rate within the plastic shock layer can be measured for a given stress amplitude $\Delta\sigma$ (stress jump across the shock front). A particular definition of the maximum strain rate ($\dot{\varepsilon}_{SG}$) was proposed by Swegle and Grady (1985) as being the ratio of the maximum time derivative of the particle velocity to the steady shock velocity. Experimental data were found by Swegle and Grady (1985) to follow closely the relationship $\dot{\varepsilon}_{SG} = B(\Delta\sigma)^{h_{SG}}$ with the exponent $h_{SG} = 4$ being nearly the same for all materials considered. These authors related h_{SG} to the material strain rate sensitivity m through the relationship, $h_{SG} = 2/m$. Thus, it was concluded that materials exhibit nearly the same strain rate sensitivity $m = 0.5$ for the deformation (strain rate) regime encountered in the shock experiments considered. Molinari and Ravichandran (2004) have obtained an analytical solution for steady state shocks of moderate intensity in metals. From

their analysis it was found that the maximum strain rate within the shock can be related to the stress jump by a power law $|\dot{\varepsilon}|_{\max} = B(\Delta\sigma)^h$ with $h = 1.87(1/m) + 0.62$ for aluminum. Therefore, for aluminum, the value $h = 4$ providing a good fit of experimental data, according to the analysis of Molinari and Ravichandran (2004), to the value m= 0.561 of the strain rate sensitivity for the high loading rates generated in shock experiments. Therefore, having a unique value of the strain rate sensitivity ($m = 0.5$ according to Swegle and Grady (1985)) for all metallic materials, is debatable.

In any case, those findings are related to the particular form of the constitutive law chosen for the modeling and more particularly to the specific form of the "nonlinear-viscous" response within the shock layer. Indeed, it is frequently assumed that the shock structure is controlled by the dissipative effects associated to the material constitutive response. However, it is well known that shocks can also be structured by dispersive effects. A good illustration is given by the Korteweg-Devries equation governing shallow water waves. In general, dispersive effects result from wave interaction with,

(i) external boundaries of the body (e.g. dispersion of elastic waves in a circular rod, Pochhammer (1876) and Chree (1889));

(ii) inner boundaries due to material heterogeneities (inclusions, layers).

In this paper, the primary faocus is on plane waves propagating in unbounded media, and therefore interactions of type (i) shall not be considered.

In the last four decades, nonlocal linear elastic laws (in particular gradient deformation theories) were formulated with the purpose of describing, within a phenomenological approach, wave dispersion related to the internal structure of heterogeneous materials, Green and Rivlin (1964), Eringen (1972, 1976), Mindlin (1964), Kunin (1982,1983), Luciano and Willis (2001).

For particular composite materials such as elastic multilayer periodic media or fiber composites, wave dispersion can be directly analyzed without using macroscopic nonlocal formulations. By considering the basic principles of continuum mechanics, wave dispersion of harmonic waves can be treated by analytical means. From the dispersion curve, the effects of elastic properties of constituents can be characterized as well as those of the geometry of the internal structure (e.g., layer's thickness of laminates), Sun et al. (1968), Achenbach (1973), Christensen (1979), Boutin (1996).

Analyses of wave dispersion in nonlinear materials accounting for the effects of internal structure are less advanced. Recently, Grady (1998) analyzed steady shock waves in polycrystalline materials and considered the possibility for shocks to be structured by dispersive effects due to wave scattering on grain boundaries. These dispersive effects were viewed as an alternative to visco-plasticity for structuring steady shock profiles. A comprehensive review of experimental work and numerical analysis of shocks in laminated materials can be found in Nesterenko (2001), Chapter 3, with a detailed discussion of transient shock waves. It is shown how the leading wave is attenuated by wave reflection at the layer's interfaces. However, as for the Korteweg-Devries equation is considered, the main signal appears finally to be the result of the competition between non-linear effects and dispersion effects, Whitham (1974).

The aim of the present work is to analyze the effects of wave dispersion on steady shock propagating in layered periodic media with nonlinear elastic or plastic properties. The direction of propagation is assumed to be perpendicular to the layers. Dispersive effects are due to wave reflection and refraction at the layer's interfaces. A detailed analysis of these interactions, which was feasible for linear elastic materials, is hard to achieve for nonlinear responses by pure analytical means, but insight can be gained through numerical simulations, Benson and Nesterenko (2001). The framework adopted here is based on a simplified constitutive assumption allowing exploring by simple calculations the structure of plastic steady shocks. It is assumed that the effect of the layered structure can be accounted for at the macroscopic level by a non-local constitutive model.

Many efforts have been recently devoted to the development of gradient plasticity theories. These approaches are aimed at accounting for the effects of the internal structure on the overall effective mechanical response, Aifantis (2003), Fleck and Hutchinson (1993, 2001), Gao et al. (1999), Huang et al. (2000). Among the different formulations developed in the literature, two gradient plasticity approaches are considered and their applicability in modeling the propagation of steady shock waves in laminates is evaluated.

The modeling of shock wave experiments, recently performed by Zhuang et al. (2002, 2003) on laminated materials, is considered here. In these experiments, the stress jump $\Delta\sigma$ across the shock and the maximum strain rate within the shock $\left|\dot{\varepsilon}\right|_{\max}$, are found to be related by a power law, $\left|\dot{\varepsilon}\right|_{\max} = B\left(\Delta\sigma\right)^{h_L}$, as for polycrystalline metals. However, the value of the exponent is now in the range $1.8 < h_L < 2.4$ depending on the specific laminate considered. These results are noticeably different from the value $h = 4$ found in shock experiments on single phase polycrystalline metals by Swegle and Grady (1985). The modeling proposed in this paper provides a quite good representation of the experimental results of Zhuang et al (2002, 2003).

2) Plastic shocks in laminates

Shock waves generated in laminate composites by planar impact, have been studied experimentally, see for example, Lundergan and Drumheller (1971) and Zhuang et al (2002, 2003). These waves propagate in the impact direction perpendicular to layers as shown in Fig. 1. The laminates considered in this paper are constituted by alternate layers of materials (1) and (2) of thickness L_1 and L_2 respectively. The elementary cell, of total thickness, $L=L_1+L_2$, is made of the two layers of dissimilar materials.

Beyond a certain propagation distance, quasi-steady plastic shocks are formed (the meaning of “quasi-steady” will be discussed later). The shock structure should depend on the properties of the constituents and also on the layer's thickness. Dispersion effects due to wave reflection and refraction at the layer’s interfaces, are thought to play a significant role in structuring the shock

front together with nonlinear effects.

The propagation distance for having steady plastic shocks depends intimately on the properties of the laminate constituents. In the experiments by Lundergan and Drumheller (1971) on steel-PMMA laminates, it was observed that, after a propagation distance *2L* of two cell sizes, the the particle velocity versus time was almost identical at. In general, at two homologous points distant by a multiple of *L* (periodicity of the internal structure) recordings of the particle velocity should be identical (up to a time shift). Observations similar to those of Lundergan and Drumheller (1971) were reported by Zhuang et al (2002, 2003) in their study of polycarbonate-steel laminates. In the experiments made by Nesterenko et al. (1983) on aluminum-copper laminates, it was shown that after a distance of *6L* no stationary wave profile was found. The higher impendence mismatch between constituents realized in metal-polymer laminates is probably a reason for having stationary shocks after a short traveling distance.

Zhuang et al. (2002, 2003) have measured the stationary propagation speed *C* of the main shock in polycarbonate-steel laminates. Let us consider now an observer moving at the constant velocity *C*. For this observer, the wave profile (spatial distribution of the particle velocity) fluctuates with a time periodicity equal to *L/C*, and a steady wave profile can be defined by time averaging over the period *L/C* of the time-fluctuating profile.

The aim of this paper is to analyze these steady shock fronts. The details of wave reflection and refraction at layer's interfaces are not analyzed. Rather the steady shock defined above by time averaging, is supposed to be representative of the dynamic response of the laminate structure after a certain propagation distance. This steady shock moves with the constant velocity *C* and maintains a constant shape.

Assuming periodicity, a steady profile can be defined in a different way. For the observer moving with the constant speed *C*, material properties are seen in average. It is thought that the average material response experienced by the observer can be identified with the macroscopic effective response of the laminate. In this paper, a phenomenological gradient plasticity approach is used to describe the effective response of the laminate, and steady shock waves are analyzed in this framework.

The constant wave profile in a steady shock is the result of the balance between steepening effects related to the non-linearity of the material response and smoothing of the wave front due to dissipative and/or dispersion effects. The dispersion effects are expected to be important in case of a large contrast between the mechanical properties of constituents**.**

For large impact velocities, the material undergoes compressive stresses beyond the initial yield limit of the constituents and a plastic shock wave is formed. Plastic shock waves have been studied in the experimental work of Zhuang et al. (2002, 2003). For a given shock strength (stress amplitude), the particle velocity was recorded in terms of time at different locations and the velocity *C* of the stationary plastic shock was measured. It was shown that the shock velocity *C* varies linearly with the particle velocity v^- measured at the rear of the plastic shock front. In addition, the maximum strain rate ($\max|\dot{\varepsilon}|$) within the shock layer was measured and the

following power law was obtained,

$$\max|\dot{\varepsilon}| = B\left(\sigma^{-}\right)^{h_L} \qquad (1)$$

where σ^{-} is the compressive stress at the rear of the plastic shock. The exponent was shown to be in the range, $1.5 < h_L < 2.2$, for the different laminates tested.

The power law (1) for a two phase laminate is similar to that of a single phase metal which, according to Swegle and Grady (1985), can be written as,

$$\max|\dot{\varepsilon}| = B\left(\Delta\sigma\right)^{h} \qquad (2)$$

where, $\Delta\sigma = \sigma^{-} - \sigma^{+}$ is the stress jump across the plastic shock (σ^{+} is the compression stress ahead of the plastic shock). Note that for the polymer-metal laminates considered here, σ^{+} is small or zero and thus $\Delta\sigma \approx \sigma^{-}$. For single phase metals, the value of the exponent h in the power law (2) was found to be close to $h \approx 4$ which is noticeably larger than values of h_L for laminates. Dispersion effects due to wave reflection and refraction at the laminate material interfaces may explain this difference. Indeed, the scope of this paper is to analyze how the shock profile can be affected by dispersion effects. In an initial analysis, dissipative effects are neglected so as to analyze the role of dispersion separately.

Laminar composites are considered, which are made of two dissimilar materials with “soft” (e.g., polymer such as polycarbonate (PC)) and “hard” (e.g., metal such as stainless steel (SS)) layers with volume fractions being respectively,

$$f_1 = L_1/L\,, \qquad f_2 = L_2/L\,. \qquad (3)$$

Material characteristics of the constituents considered in the modeling are given in Table 1.

Two different composites are obtained by varying the layer’s thickness. The PC37/SS19 laminate corresponds to $L_1 = 0.37\ mm$ and $L_2 = 0.19\ mm$ and PC74/SS37 is obtained by doubling the width of layers.

Experimental data (Zhuang et al. (2002, 2003)) plotted in Fig. 2 show that the Lagrangian shock speed is related to the particle velocity v^{-} at the rear of the shock by a linear relationship. For plastic shocks of moderate amplitude, this linear relationship can be written as:

$$C = c^{+} + S(v^{-} - v^{+}) \qquad (4)$$

where the subscript (+) refers to the state ahead of the plastic shock; v^+ is the particle velocity ahead of the shock front and c^+ is the sound velocity corresponding to state (+).

Note that the experimental data shown in Fig. 2 provide identical linear relationships for both composites, showing no sensitivity to the cell size. The sensitivity of the shock wave profile to the cell size is analyzed in Nesterenko (2001). For solid teflon-paraffin laminates, Nesterenko et al. (1983) report that the amplitude of the particle velocity, at a distance of *2L* or *4L* from the impact plane, is nearly insensitive to the cell size. It is believed that this independence with respect to cell size, as in the experiments of Zhuang et al. (2002, 2003), is a feature of steady shocks. For transient shock profiles there is a strong effect of the cell size on the amplitude of the leading signal, see Nesterenko (2001) Fig. 3.6 for aluminum-copper laminate.

The slope of the best fit lines for the experimental data in Fig. 2 is given by,

$$S = 2.1 \qquad (5)$$

The relationship (4) with S=2.1, $v^+ = 18.2\ m/s$ (value determined later) and $c^+ = 1{,}600\ m/s$ shows a good fit with the experimental data. Note that the Hugoniot curve of the laminate can be obtained from (4), for further discussion, see section 4.

3) Basic equations

A Lagrangian formulation is used to account for the large uniaxial deformations occurring in shock wave experiments. The direction of propagation of the plane wave is denoted by Ox, Fig. 1; *u* is the component of the displacement in this direction, other components along directions *y* and *z* being equal to zero. The orthogonal frame *Oxyz* has unit vectors $\underline{e}_1$, $\underline{e}_2$ and $\underline{e}_3$. Note that the stresses and deformations considered in the following are defined at the macroscopic level of the composite.

The present position *x* of a particle is given by:

$$x = X + u(X) \qquad (6)$$

where *X* is the initial position prior to any deformation. The deformation gradient has the form,

$$\underline{F} = \lambda_1 \underline{e}_1 \otimes \underline{e}_1 + \underline{e}_2 \otimes \underline{e}_2 + \underline{e}_3 \otimes \underline{e}_3 \qquad (7)$$

where the longitudinal stretch is,

$$\lambda_1 = \frac{\partial x}{\partial X} = 1 + \frac{\partial u}{\partial X} \qquad (8)$$

The standard multiplicative decomposition of $\underline{F}$ into elastic (e) and plastic parts (p) , see Fig. 3, can be written as,

$$\underline{F} = \underline{F}^e \underline{F}^p \qquad (9)$$

with

$$\underline{F}^e = \lambda_1^e \underline{e}_1 \otimes \underline{e}_1 + \lambda_2^e \underline{e}_2 \otimes \underline{e}_2 + \lambda_2^e \underline{e}_3 \otimes \underline{e}_3 \qquad (10)$$

$$\underline{F}^p = \lambda_1^p \underline{e}_1 \otimes \underline{e}_1 + \lambda_2^p \underline{e}_2 \otimes \underline{e}_2 + \lambda_2^p \underline{e}_3 \otimes \underline{e}_3 \qquad (11)$$

Note that $\lambda_2^e = \lambda_3^e$ and $\lambda_2^p = \lambda_3^p$ due to the rotational symmetry around the direction $\underline{e}_1$.

The condition of plastic incompressibility:

$$\lambda_1^p (\lambda_2^p)^2 = 1 \qquad (12)$$

and the multiplicative decomposition (9) provide three independent relations relating the stretches λ_1, λ_1^e, λ_2^e, λ_1^p and λ_2^p. Therefore all stretches can be expressed in terms of λ_1 and λ_1^p,

$$\lambda_1^e = \lambda_1 / \lambda_1^p, \qquad \lambda_2^e = (\lambda_1^p)^{1/2}, \quad \lambda_2^p = (\lambda_1^p)^{-1/2}. \qquad (13)$$

Denoting by $\underline{T}$ the nominal stress tensor with respect to the initial configuration C_0, one has, Clifton (1971), Lubarda (2002):

$$\underline{T} = (\underline{F}^p)^{-1}.\underline{T}^e \qquad (14)$$

The elastic constitutive law is expressed in the intermediate configuration C_r, Fig. 3, as:

$$\underline{T}^e = \frac{\partial \psi^e}{\partial \underline{F}^e} \qquad (15)$$

where ψ^e is the macroscopic elastic strain energy (volume average of the layer's strain energy). From (11) and (14),

$$T_{11} = \frac{T_{11}^e}{\lambda_1^p} \qquad (16)$$

To represent the nonlinear elastic response for compressive loading, the elastic law (15) should include higher order elastic coefficients. Second order elastic coefficients can be characterized by ultrasonic measurements; however this information is not available for the laminates studied here. Therefore second order elastic constants will be introduced as parameters, and a parametric analysis will be performed to quantify how results are affected by second order elastic constants.

The following nonlinear constitutive law is adopted,

$$T_{11}^e = (C_{1111}\varepsilon_1^e + 2C_{1122}\varepsilon_2^e)(1 - b(\varepsilon_1^e + 0.2\varepsilon_2^e)) \qquad (17)$$

where C_{1111} and C_{1122} are components of the overall (effective) linear elastic moduli of the laminate. For both laminates PC37/SS19 and PC74/SS37, one has the same values:

$$C_{1111} = 6.84\ GPa\,, \qquad C_{1122} = 3.60\ GPa\,. \tag{18}$$

Second order elastic properties are scaled by, b=66.7 . This value will be varied in the parametric analysis.

Elastic deformations ε_1^e and ε_2^e are expressed in terms of λ_1 and λ_1^p by,

$$\varepsilon_1^e = \log(\lambda_1^e) = \log(\lambda_1 / \lambda_1^p)$$

$$\varepsilon_2^e = \log(\lambda_2^e) = \frac{1}{2}\log(\lambda_1^p) \tag{19}$$

Combining (16), (17) and (19), the stress component T_{11}, denoted henceforth for simplicity as T, can be written in terms of λ_1 and λ_1^p,

$$T = T(\lambda_1, \lambda_1^p)\,. \tag{20}$$

The compressive stress (with positive sign) is defined as follows,

$$\sigma = -T\,. \tag{21}$$

4) Steady plastic shocks and the Hugoniot

Plate impact experiments are consdiered, where stationary plastic shocks are formed beyond a certain propagation distance. These shocks move with constant speed and constant shape. Two cases are considered,

(i) the stress amplitude exceeds the elastic limit of the composite so as to form a plastic shock preceded by an elastic precursor with higher propagation speed;

(ii) the stress amplitude is sufficiently large to form a single elasto-plastic shock.

The analysis is restricted to weak shocks, i.e., temperature effects are neglected and the process is considered as isentropic, see Clifton (1971) and Molinari and Ravichandran (2004) for further comments.

4.1) Plastic shock with elastic precursor

For moderate impact velocities, the plastic shock is preceded by an elastic precursor where the material is compressed from the initial state (0) to state (+) corresponding to first plastic yielding. The values of stress, particle velocity and stretches associated to state (+) are denoted by $\sigma^+ = -T^+, v^+$, λ^+ and λ^{p+}, where the subscript (1) has been dropped to simplify the notation. In the plastic shock, the material is further compressed to state (-) with stress

$\sigma^- = -T^-$ reached at the rear of the plastic front, see Fig. 4. The transition between states (+) and (-) occurs within the plastic shock front, a thin layer where the material sustains high strain rates.

The equation of conservation of momentum is,

$$\frac{\partial T}{\partial X} = \rho_0 \frac{\partial v}{\partial t} \tag{22}$$

where t is time, $v = \partial u(X,t)/\partial t$ is the particle velocity and ρ_0 is the mass density in the reference configuration, C_0. The compatibility equation has the form,

$$\frac{\partial v}{\partial X} = \frac{\partial \lambda}{\partial t}. \tag{23}$$

For an observer moving with the plastic shock velocity C, the problem is steady and all variables can be expressed in terms of the parameter,

$$\xi = x - Ct \tag{24}$$

with states (+) and (-) corresponding respectively to $\xi = +\infty$ and $\xi = -\infty$.

Using (24), the equations (22) and (23) are written as,

$$\frac{\partial T}{\partial \xi} = -C\rho_0 \frac{\partial v}{\partial \xi} \tag{25}$$

$$\frac{\partial v}{\partial \xi} = -C \frac{\partial \lambda}{\partial \xi}. \tag{26}$$

Upon integration, it can be shown that any state within the plastic shock layer has to satisfy the following relationships,

$$T - T^+ = -\rho_0 C(v - v^+) \tag{27}$$

$$v - v^+ = -C(\lambda - \lambda^+) \tag{28}$$

By combining (27) and (28) the equation defining the Rayleigh line is obtained (see Fig. 4),

$$T - T^+ = \rho_0 C^2(\lambda - \lambda^+) \tag{29}$$

In particular, state (-) is related to state (+) by,

$$T^- - T^+ = -\rho_0 C(v^- - v^+) \tag{30}$$

$$v^- - v^+ = -C(\lambda^- - \lambda^+) \tag{31}$$

$$T^- - T^+ = \rho_0 C^2(\lambda^- - \lambda^+)\,. \qquad (32)$$

The Hugoniot is the curve defined by the ensemble of points (σ^-, λ^-) obtained by varying the stress amplitude σ^-, Fig. 4. The intercept of the elastic-loading curve $\lambda \rightarrow T(\lambda, \lambda^p = 1)$ with the Hugoniot is the state (+), see Fig. 4. Thus, the compressive stress σ^+ at state (+) follows the following relationship,

$$\sigma^+ = -T(\lambda^+, 1)\,. \qquad (33)$$

The state (+) is also defined as being the initial yield limit of the composite. It will be shown that the precise characterization of state (+) is not a crucial point. This is related to the fact that, for the metal-polymer composite studied here, the value of the initial yield limit is small and does not affect the results. Therefore, a conventional definition of state (+) can be adopted by setting $\lambda^+ = 0.99$, see Fig. 4. The corresponding stress is σ^+=0.115GPa. The particle velocity at state (+) is given by (see for instance Molinari and Ravichandran (2004)),

$$v^+ = c_{el}(1 - \lambda^+) \qquad (34)$$

where

$$c_{el} = \sqrt{\frac{\sigma^+}{\rho_0(1 - \lambda^+)}} \qquad (35)$$

is the velocity of the elastic precursor. ρ_0 is the average mass density of the composite in the reference configuration:

$$\rho_0 = f_1\,\rho_1 + f_2\,\rho_2\,. \qquad (36)$$

The two PC-SS laminates differ only by a factor two in the layer's thickness; therefore they have same mass density $\rho_0 = 3{,}468\ kg/m^3$. The elastic compression curve is also identical and the initial yield limit is reached for the same value of the nominal stress denoted by T^+. Both composites have the same state (+). The particle velocity at the rear of the elastic shock is $v^+ = 18.2\ m/s$. The velocity of the elastic shock precursor is $c_{el} = 1{,}820\ m/s$.

By substituting (31) into (4),

$$C = \frac{c^+}{1 - S(\lambda^+ - \lambda^-)} \qquad (37)$$

which upon substitution into (32) provides,

$$\sigma^- = \sigma^+ + \frac{\rho_0 c^{+2}(\lambda^+ - \lambda^-)}{(1 - S(\lambda^+ - \lambda^-))^2} \tag{38}$$

The Hugoniot curve gives the value of the "equilibrium" compressive stress σ_H reached behind the plastic shock in terms of the stretch λ,

$$\sigma_H(\lambda) = \sigma^+ + \frac{\rho_0 c^{+2}(\lambda^+ - \lambda)}{(1 - S(\lambda^+ - \lambda))^2} \tag{39}$$

The value of the equilibrium stress can be maintained under static compression by keeping fixed values of the state variables (λ, λ^p and temperature). The Hugoniot curve is displayed in Fig. 5 for λ^+=0.99 and $c^+ = 1600 m/s$, for stress amplitudes up to 9 GPa. From the experimental data shown in Fig. 2, c^+ is determined using (4) by setting c^+=C at $\nu^- = \nu^+$. The values of parameters S, ρ_0 and c^+ entering into the expression (39) of the Hugoniot, are given in Table 2.

For a given stress amplitude σ^-, the corresponding point on the Hugoniot is associated to the stretch λ^- defined by,

$$\sigma^- = \sigma_H(\lambda^-). \tag{40}$$

The configuration of a plastic shock with an elastic precursor is physically realizable if the velocity c_{el} of the elastic precursor is larger than the plastic shock velocity C,

$$c_{el} = \sqrt{\frac{\sigma^+}{\rho_0(1-\lambda^+)}} \geq C = \sqrt{\frac{\sigma^- - \sigma^+}{\rho_0(\lambda^+ - \lambda^-)}}. \tag{41}$$

The case where this condition is not satisfied (shocks of larger amplitude) is studied in the next section.

Note that the analytical form (39) of the Hugoniot was derived by considering shocks of weak enough stress amplitude. It is assumed in the following that the Hugoniot can be described in first approximation by the same expression (39) extrapolated to a larger range of stress amplitude. The consistency of this hypothesis will be validated by comparing the prediction of the theory with a different set of experimental data.

4.2) Case of a single elastic-plastic shock

When the condition (41) is not satisfied, an unique shock is formed, relating the initial state (0) to the state (-) as shown in Fig. 6 for the stress amplitude, $\sigma^- = 2GPa$. The Rayleigh line is given by (29) where the state (+) is replaced by state (0),

$$T = \rho_0 C^2(\lambda - 1). \qquad (42)$$

The intercept of the Rayleigh line with the elastic loading path $\lambda \to \sigma = -T(\lambda, \lambda^p = 1)$ defines the state (*). States (0) and (*) are related by a pure elastic path. Plastic flow occurs between states (*) and (-).

The shock velocity is given by (42),

$$C = \sqrt{\frac{\sigma^-}{\rho_0(1-\lambda^-)}}. \qquad (43)$$

Figure 2 shows the shock velocity C in terms of the particle velocity v^- at the rear of the shock. Experimental data are represented by stars for PC37/SS19 and by squares for PC74/SS37. The modeling prediction corresponds to the solid line with dots representing different levels of the applied stress σ^- (from 1 GPa to 9 GPa). For given values of σ^-, the theoretical results have been obtained by calculating λ^- with (39) and (40). The values of material characteristics in (39) are given in Table 2. The shock velocity *C* is obtained with (43) and v^- with (31) where state (+) is replaced by the initial state (0), $v^- = -C(\lambda^- - 1)$. Good quantitative agreement is found in Fig. 2 with respect to experimental data (given in Table 3). The relationship (4), with $v^+ = 18.2\ m/s$ and $c^+ = 1{,}600\ m/s$ provides results (dashed line) which are very close to those predicted by using the expression (39) of the Hugoniot extrapolated to large stresses (up to 10 GPa). This comparison provides a first validation of the foregoing extrapolation.

5) Structure of plastic shocks in laminates

For stress amplitude σ^- larger than 1 GPa, the relationship (41) is not satisfied, and states (0) and (-) are related by a single shock as shown in Fig. 6, composed of an elastic jump from state (0) to (*) and plastic shock from state (*) to (-). The value of the stretch λ^* at state (*) corresponds to the intercept of the Rayleigh line (42) with the elastic path $\lambda \to \sigma = -T(\lambda,1)$

emanating from state (0).

$$\frac{\sigma^{-}(\lambda^{*}-1)}{\lambda^{-}-1} = -T(\lambda^{*},1) \qquad (44)$$

For the amplitude $\sigma^{-} = 2$ MPa , the following values are found, $\lambda^{*} = 0.981$ $\sigma^{*} = 0.28$ MPa .

Consider now any point on the Rayleigh line between states (*) and (-) i.e., for $\lambda^{-} \le \lambda \le \lambda^{*}$. For each point there is a one-to-one correspondence between λ and the plastic stretch λ^{p} in the interval $\lambda^{p-} \le \lambda^{p} \le 1$. This correspondence is given by,

$$T_1(\lambda, \lambda^{p}) = \rho_0 C^2(\lambda - 1) . \qquad (45)$$

which can be resolved into,

$$\lambda = g_R(\lambda^{p}) . \qquad (46)$$

Similarly, on the Hugoniot, there is a one-to-one correspondence between λ and λ^{p} denoted as,

$$\lambda = g_H(\lambda^{p}) \qquad (47)$$

For a given value of the plastic stretch λ^{p} , consider the intersections (I_R) and (I_H) of the elastic path $\lambda \to \sigma = -T(\lambda, \lambda^{p})$ with the Rayleigh line and the Hugoniot, respectively, see Fig. 7. Note that the same value of the plastic stretch λ^{p} is associated with I_H and I_R , and that $\lambda = g_H(\lambda^{p})$ for I_H and $\lambda = g_R(\lambda^{p})$ for I_R .

The compressive stress $\sigma_{I_H} = -T(g_H(\lambda^{p}), \lambda^{p})$ associated with I_H is the yield stress obtained at the rear of the plastic front in a plate impact experiment with stress amplitude σ_{I_H} . Therefore, this yield stress can be associated to a state of homogeneous plastic deformation defined by the plateau behind the plastic shock. However, within the shock structure the plastic deformation is highly non-uniform. For these high plastic deformation gradients, conventional plasticity laws are not able to restitute properly the overall material response, in particular when the shock-width is comparable to the characteristic lengths of the composite internal structure. To

account for the interaction between the internal structure and the propagating wave, it is appealing to consider a nonlocal plasticity theory.

Nonlocal theories of plasticity have been developed in the last two decades to formulate macroscopic phenomenological laws taking into account the effects of the material internal structure, see for example, Aifantis (2003), Fleck and Hutchinson (1993, 2001), Gao et al. (1999), Huang et al. (2000). Our aim here is to model geometrical dispersion in laminate media by using nonlocal plasticity models. Two gradient plasticity formulations and their predictions are compared.

Dissipation of mechanical work into heat by viscosity can also contribute together with dispersion effects to the build-up of the shock structure. To separate these effects, viscous dissipation will not be considered here.

5.1) First order gradient plasticity approach

In this section, a first order gradient plasticity approach is considered. Such theories have been recently developed in the context of polycrystalline materials, the internal characteristic length being of the order of the grain size (about $10\mu m$), Fleck and Hutchinson (1993,2001), Gao et al. (1999), Huang et al (2000). For the laminated media considered here, the internal length is expected to be scaled by the layer widths.

In the first order gradient plasticity theory used here, the yield stress σ_Y is a function of the accumulated plastic strain $\bar{\varepsilon}^p$ and of the first gradient of this strain. It is assumed that,

$$\sigma_Y = \sigma_{Y0}(\bar{\varepsilon}^p) + \kappa\left|\partial\bar{\varepsilon}^p / \partial x\right|^\beta \qquad (48)$$

In the compression tests under consideration $\bar{\varepsilon}^p$ can be identified to the opposite of the longitudinal plastic strain.

$$\bar{\varepsilon}^p = -\varepsilon^p = -\log(\lambda^p) \qquad (49)$$

κ and β are positive material parameters which are related to the internal structure of the laminate (geometry of the layers, material characteristics of the constituents, including the mass densities since the impedance mismatch between layers plays a role in wave reflection and refraction).

The yield stress σ_Y corresponding to the state I_R differs from the yield stress σ_{Y0} associated with the state I_H on the Hugoniot, the latter being related to a state of homogeneous deformation. In the present modeling, the gap between these yield stresses is

attributed to the high level of heterogeneity of plastic deformation in the shock front. The yield stress is assumed to be affected by the plastic strain gradient as in (48),

$$\sigma_{I_R} = \sigma_{I_H} + \kappa \left| \partial \bar{\varepsilon}^p / \partial x \right|^{\beta} \tag{50}$$

with,

$$\sigma_{I_H} = -T(g_H(\lambda^p), \lambda^p), \qquad \sigma_{I_R} = -T(g_R(\lambda^p), \lambda^p). \tag{51}$$

Defining the function,

$$\hat{f}(\bar{\varepsilon}^p) = \left(\frac{1}{\kappa}(-T(g_R(\lambda^p), \lambda^p) + T(g_H(\lambda^p), \lambda^p))\right)^{1/\beta} \tag{52}$$

where $\lambda^p = \exp(\varepsilon^p) = \exp(-\bar{\varepsilon}^p)$, (50) can be rewritten as,

$$\frac{\partial \bar{\varepsilon}^p}{\partial x} = -\hat{f}(\bar{\varepsilon}^p). \tag{53}$$

The sign (-) comes from the fact that $\bar{\varepsilon}^p$ is a decreasing function of *x* for a wave moving to the right. Note that the plastic deformation varies within the shock from $\bar{\varepsilon}^{p*}=0$ (state *) to $\bar{\varepsilon}^{p-} = -\log(\lambda^{p-})$ (state -) and that $\hat{f}(\bar{\varepsilon}^p)$ vanishes for state (-).

Upon integration of (53) between state (*) and state (-), the shock profile can be obtained for the particle velocity, the total strain $\varepsilon = \log(\lambda)$ and the cumulated plastic strain $\bar{\varepsilon}^p = -\log(\lambda^p)$.

All numerical calculations in the following are made for a linear dependence of the yield stress upon the plastic strain gradient, i.e., for $\beta = 1$, and a good correspondence with experimental results is found for that value of β. However, in general β can have any positive value and the effect obtained by varying the value of β will be considered later when discussing second gradient plasticity approaches.

Figure 8 shows the profile of $\bar{\varepsilon}^p$ within the shock and the variation of $\hat{f}(\bar{\varepsilon}_p)$. Calculation were made for the stress amplitude $\sigma^- = 2$ GPa and $\kappa = 1.7$ m MPa, $\beta = 1$. A smooth transition is observed when $\xi \to -\infty$. On the contrary the value $\bar{\varepsilon}^p = 0$ corresponding to state (*) is reached at a finite value of ξ and for a non-zero value of the slope $\partial \bar{\varepsilon}^p / \partial \xi$.

Note that according to the present modeling, there is no elastic precursor. This is in

agreement with experimental observations of Zhuang et al (2003).

An important role in structuring the shock is played by the parameter κ which accounts for the internal structure of the laminate. From (48) it follows that κ has the dimension of $(\text{length})^{\beta}$ x (stress). Considering that κ is a function of the layer's geometry (specified by L_1 and $L=L_1+L_2$) and its material properties, and using dimensional analysis (Vaschy-Buckingham theorem), it is easily found that,

$$\kappa(L^{\beta}\sigma_{ref})^{-1} = F(L_1/L, \text{non-dimensional material parameters}) \qquad (54)$$

F is a non-dimensional quantity and σ_{ref} is any characteristic stress, for instance the elastic shear modulus of phase 1. Non-dimensional material parameters are of the form: λ_1/σ_{ref}, μ_1/σ_{ref}, λ_2/σ_{ref}, μ_2/σ_{ref}, σ_{Y1}/σ_{ref}, n_1, σ_{Y2}/σ_{ref}, n_2, ρ_1/ρ_2, where λ_i, μ_i, σ_{Yi}, n_i are for phase (i) respectively: the two Lamé constants, the initial yield stress and the hardening exponent (if a power law of Hollomon or Ramberg-Osgood type is assumed to describe strain hardening of a given constituent). Note that mass densities ρ_1 and ρ_2 of constituents are involved through the effect of the impedance mismatch in reflection and refraction of waves at interfaces beteen different phases. Mass densities are combined in the ratio ρ_1/ρ_2. Therefore, for a given volume fraction $f_1=L_1/L$ of phase 1, κ appears to be proportional to L^{β} based on (54).

For the stress amplitude $\sigma^- = 2$ GPa and for $\kappa = 1.7$ m Mpa, $\beta = 1$, the shock width can be evaluated approximately as 0.5 mm from Fig. 8. A direct estimate of the shock width is obtained from the relationship,

$$w = \frac{\left|\varepsilon^{p-}\right|}{\left|\partial\varepsilon^{p}/\partial\xi\right|_{\max}} = C\frac{\left|\varepsilon^{p-}\right|}{\left|\dot{\varepsilon}^{p}\right|_{\max}} \qquad (55)$$

where $\left|\dot{\varepsilon}^{p}\right|_{\max}$ is the maximum plastic strain rate within the shock layer. From (53), $\left|\partial\varepsilon^{p}/\partial\xi\right|_{\max} = \max_{0\le\bar{\varepsilon}^{p}\le\bar{\varepsilon}^{p-}}(\hat{f}(\bar{\varepsilon}^{p}))$. Note also that $\left|\dot{\varepsilon}^{p}\right|_{\max} = C\left|\partial\varepsilon^{p}/\partial\xi\right|_{\max}$. For $\sigma^- = 2$ GPa the shock width in PC37/SS19 is estimated using (55) as w=0.49 mm in agreement with the shock profile shown in Fig. 8. Note that w is comparable to the cell size L=0.56 mm.

For a given volume fraction of constituents, the following relationships between the internal structure of the composite material and the shock structure can be demonstrated:

$$\kappa \propto L^{\beta}, \qquad \left|\dot{\varepsilon}^{p}\right|_{\max} \propto \frac{1}{L}, \quad w \propto L \tag{56}$$

The proportionality of κ with respect to L^{β} results from (54). By using (53) one obtains $\dot{\bar{\varepsilon}}^{p} = C\frac{\partial \bar{\varepsilon}_{p}}{\partial \xi} = -C\hat{f}(\bar{\varepsilon}_{p})$, and from the dependence $\kappa \propto L^{\beta}$, it follows with (52) that $\left|\dot{\varepsilon}^{p}\right|_{\max} \propto \kappa^{-1/\beta} \propto \frac{1}{L}$. Finally, with (55), the width of the shock layer appears to be proportional to L, irrespective of the value of the exponent β.

In Fig. 9 the stress amplitude is displayed in terms of $\left|\dot{\varepsilon}^{p}\right|_{\max}$ in a log-log diagram, for $\beta = 1$. Results of the model, given by the solid line for PC37/SS19 and by the dashed line for PC74/SS37, reproduce quite well the experimental data. Theoretical predictions are obtained by using material characteristics given in Tables 2 and 4.

PC37/SS19 and PC74/SS37 laminates have same proportion of constituents, i.e., same volume fractions. The only difference between those laminates is the layer's total thickness which is double for PC74/SS37 in comparison to PC37/SS19. The cell size has the value $L = 0.56\ mm$ for PC37/SS19 and $L \cong 1.12\ mm$ for PC74/SS37. For a fixed value of the volume fraction f_1 and for $\beta = 1$, κ is proportional to L, according to (54). Therefore, the value $\kappa = 3.4x10^{6}\ m.Pa$ for PC74/SS37 is taken to be twice the value $\kappa = 1.7x10^{6}\ m.Pa$ for PC37/SS19. Since by (56), $\left|\dot{\varepsilon}^{p}\right|_{\max} \propto 1/\kappa \propto 1/L$, the strain rate $\left|\dot{\varepsilon}^{p}\right|_{\max}$ for a given stress amplitude σ^{-}, has a value twice larger for PC37/SS19 than for PC74/SS37. This is in agreement with experimental data shown in Fig. 9.

Results in Fig. 9 can be used to represent both laminates through the following power law:

$$\left|\dot{\varepsilon}^{p}\right|_{\max} = B\left(\sigma^{-}\right)^{h_L} \tag{57}$$

with $h_L = 1.82$. It can be shown that the slope $1/h_L$ of the lines in Fig. 9 does not depend upon κ but is a function of β (this will be further discussed when considering second gradient plasticity theories). However, for a given value of β, the position of those lines does depend on κ. Note that the first gradient theory with a linear dependence of the yield stress upon the plastic

strain gradient ($\beta = 1$) provides a good prediction of $1/h_L$ together with the appropriate effect of the cell size on strain rates. The value of κ for the PC37/SS19 laminate was calibrated so as to get the best fit with experimental results ($\kappa = 1.7\ m.MPa$). The comparison with experimental results for PC74/SS37, Fig. 9, shows a quite good agreement and furnish an additional check of the pertinence of the present modelling. Indeed, it is worth mentioning that experimental results in Fig. 9, obtained for two laminates subjected to various shock intensities, have been described for $\beta = 1$, with a single calibration of the parameter κ for one of the laminates, the value of κ for the second laminate being deduced from the theory ($\kappa = 3.4\ m.MPa$ for PC74/SS37which is twice larger than for PC37/SS19).

The total strain rate within the shock can be estimated as the ratio of the total strain variation across the shock ε^- by the rise time, w/C,

$$\tilde{\dot{\varepsilon}} = C\left|\varepsilon^-\right|/w \tag{58}$$

Using the estimate (54) of the shock width,

$$\tilde{\dot{\varepsilon}} = \frac{\varepsilon^-}{\varepsilon^{p-}}\left|\dot{\varepsilon}^p\right|_{\max} \tag{59}$$

In Fig. 10 the dependence of the stress amplitude σ^- upon $\left|\dot{\varepsilon}^p\right|_{\max}$ and $\tilde{\dot{\varepsilon}}$ is shown in a log-log diagram. A small shift towards larger strain rate is obtained when considering $\tilde{\dot{\varepsilon}}$. However the value h_L=1.82, which characterizes the slope, is essentially left unchanged. The small difference between the results of Fig. 10, presented either in terms of the total strain rate or in terms of the plastic strain rate, justify that no distinction is made in the discussion between the representations (1) and (57).

Figure 11 shows the evolution of the shock width w in terms of the stress amplitude σ^- for PC37/SS19 and PC74/SS37 laminates. Since the volume fraction of constituents is identical for the two laminates, w is proportional to L (0.56 mm for PC37/SS19, twice larger for PC74/SS37). Thus for a given stress amplitude, w is twice larger for PC74/SS37.

The use of a nonlocal constitutive law such as the one proposed in (50) is of interest when the characteristic length of stress (or strain) heterogeneity (which can be identified here with the width of the shock layer w) is of the order of the characteristic lengths L_1 and L_2 defining the laminate's internal structure. Considering for instance the PC37/SS19

laminate, values of w (from 0.984 mm at σ^-=1GPa to 0.091 mm at σ^-=10GPa) are comparable to $L_1 = 0.37\ mm$ and $L_2 = 0.19\ mm$.

The effect of second order elastic constants is on the results is shown in Fig. 12(a) where the stress amplitude σ^- is reported in terms of the maximum of the plastic strain rate $\left|\dot{\varepsilon}^p\right|_{\max}$ (log-log diagram). In the elastic law (17), second order elastic constants are scaled by the parameter *b*. Previous results obtained for the value *b*=66.7 (solid line) are compared with those for *b*=100 (dashed line). A little shift and a small change in the slope are obtained between the two lines representing results for b=66.7 and b=100. Similar trends were obtained when analyzing shock waves in polycrystalline metals, see Fig. 15 in Molinari and Ravichandran (2004).

The effect of λ^+ (defining the state (+)) is shown in Fig. 12(b). The solid line corresponds to the previous results of Fig. 9 (σ^- versus $\left|\dot{\varepsilon}^p\right|_{\max}$ with λ^+=0.99). Two different curves are shown for λ^+=0.97. The solid line with dots represents σ^- in terms of $\left|\dot{\varepsilon}^p\right|_{\max}$ The dashed line shows the variation of the stress jump $\Delta\sigma = \sigma^- - \sigma^+$ with respect to $\left|\dot{\varepsilon}^p\right|_{\max}$. This result indicates that the effect of λ^+ is almost negligible when considering variations of $\Delta\sigma$ in terms of $\left|\dot{\varepsilon}^p\right|_{\max}$. Note that for λ^+=0.99, σ^+=0.115GPa is negligible with respect to σ^- for the range of stress amplitudes considered here; thus $\sigma^- \approx \Delta\sigma$. However, this is not the case for λ^+=0.97, for which $\sigma^+ = 0.631\,\text{GPa}$. From this discussion, it can be concluded that results presented in Fig. 9 would only be slightly affected by considering values of λ^+ smaller than 0.99.

5.2) Second order gradient plasticity approach

Second order gradient plasticity approaches are frequently used in the literature to analyze strain localization phenomena, for example, Aifantis (2003). In this section the pertinence of such constitutive modeling with respect to shock wave analysis in laminate media is evaluated.

The yield stress σ_Y which was given by (48) for the first order gradient approach is presently assumed to be dependent upon the second gradient of the accumulated plastic strain,

$$\sigma_Y = \sigma_{Y0}(\bar{\varepsilon}_p) + \kappa_1 \left| \frac{\partial^2 \bar{\varepsilon}^p}{\partial x^2} \right|^{\beta_1} \tag{60}$$

where κ_1 and β_1 are positive material parameters accounting for the laminate internal structure. The relationships (50) and (53) are replaced by,

$$\sigma_{I_R} = \sigma_{I_H} + \kappa_1 \left| \frac{\partial^2 \bar{\varepsilon}^p}{\partial x^2} \right|^{\beta_1} \tag{61}$$

and

$$\frac{\partial^2 \bar{\varepsilon}^p}{\partial x^2} = \hat{f}_1(\bar{\varepsilon}^p) \tag{62}$$

with

$$\hat{f}_1(\bar{\varepsilon}^p) = \left(\frac{1}{\kappa_1}(-T(g_R(\lambda^p), \lambda^p) + T(g_H(\lambda^p), \lambda^p))\right)^{1/\beta_1} . \tag{63}$$

First quadrature of (62) can be obtained by multiplying both sides by $\frac{\partial \bar{\varepsilon}^p}{\partial x}$. Upon integration from state (*) to the present state, and assuming a smooth transition at state (*), i.e., $\left.\frac{\partial \bar{\varepsilon}^p}{\partial x}\right|_* = 0$, and a negative slope $\frac{\partial \bar{\varepsilon}^p}{\partial x} < 0$ elsewhere in the shock layer, one obtains,

$$\frac{\partial \bar{\varepsilon}^p}{\partial x} = -\sqrt{2\hat{g}(\bar{\varepsilon}^p)} \tag{64}$$

with

$$\hat{g}(\bar{\varepsilon}^p) = \int_0^{\bar{\varepsilon}^p} \hat{f}_1(\varsigma) d\varsigma \tag{65}$$

For the stress amplitude $\sigma^- = 2$ GPa, Fig. 13 shows how shock profiles compare for the first gradient and second gradient plasticity theories, defined by (48) and (60),respectively with parameters ($\kappa = 1.7$ m.MPa, $\beta = 1$) and ($\kappa_1 = 750$ m^2.Pa, $\beta_1 = 1$). For the second gradient model,

a smooth transition to $\bar{\varepsilon}^p = 0$ is observed when ξ increases. On the contrary the value $\bar{\varepsilon}^{p-}$=0.118 corresponding to state (-) is reached at a finite value of ξ beyond which an homogeneous state is obtained. The reverse situation is observed for the first gradient theory; the state (-) being reached asymptotically when $\xi \to -\infty$, while the state (*) corresponds to a finite value of ξ with a slope different from zero.

In Fig. 14 the profiles of plastic strain $\bar{\varepsilon}^p$ and the magnitude of total strain $|\varepsilon| = |\log(\lambda)|$ are shown for the second gradient approach ($\kappa_1 = 750\ \mathrm{m}^2.\mathrm{Pa}$, $\beta_1 = 1$). The stress amplitude is $\sigma^- = 2\ \mathrm{GPa}$. At the shock front, there is an elastic jump from state (0) to state (*), see Fig. 6. Thus, the total strain is discontinuous at the shock front, while the plastic strain is continuous and equal to zero.

The parameter κ_1 in (60), accounting for the effect of the laminate's internal structure on the constitutive response, follows the following relationship obtained from dimensional analysis,

$$\kappa_1 (L^{2\beta_1} \sigma_{ref})^{-1} = F(L_1 / L, \text{non - dimensional material parameters}) \qquad (66)$$

It appears that, for a given volume fraction of constituents, κ_1 is proportional to $L^{2\beta_1}$. Note that for the first gradient model, κ was found to be proportional to L^{β}.

The shock width w_1 can be estimated by using (55) and (64). Thus, it is found that,

$$\left| \frac{\partial \varepsilon^p}{\partial \xi} \right|_{\max} = \sqrt{2\hat{g}(\bar{\varepsilon}^{p-})} \qquad (67)$$

and

$$w_1 = \frac{\left|\varepsilon^{p-}\right|}{\left|\partial \varepsilon^p / \partial \xi\right|_{\max}} = \left|\varepsilon^{p-}\right| \Big/ \sqrt{2\hat{g}(\bar{\varepsilon}^{p-})}\,. \qquad (68)$$

For the PC37/SS19 laminate with $\kappa_1 = 750\ \mathrm{m}^2.\mathrm{Pa}$ and $\beta_1 = 1$, the shock width w_1=0.385 mm is obtained from (68) for $\sigma^- = 2\ \mathrm{GPa}$.

For a given volume fraction of constituents, it follows immediately from the definition (65) of $\hat{g}$ and from the dependence $\kappa \propto L^{2\beta_1}$ that,

$$w_1 \propto L\,, \quad \left|\dot{\varepsilon}^p\right|_{\max} \propto \frac{1}{L} \tag{69}$$

The scaling of the shock width and of the magnitude of plastic strain rate by the laminate cell size L, is similar to the scaling obtained in (56) with the first gradient theory.

The major difference between the two gradient plasticity approaches appears when looking at the dependence of the stress amplitude σ^- upon $\left|\dot{\varepsilon}^p\right|_{\max}$ shown Fig. 15. Compared to experimental results of PC37/SS19, it appears that the slope $1/h_L$ is not adequate for the second gradient model with $\beta_1 = 1$ (linear dependence of the yield stress upon the second gradient of the plastic deformation).

Figure16 illustrates the effects of parameters β_1 and κ_1 on the relationship between stress amplitude and magnitude of the plastic strain rate. For a given value of (β_1, κ_1) this relationship is fairly well represented in the log-log diagram of Fig. 16 by a straight line denoted by $\mathsf{L}(\beta_1, \kappa_1)$ with slope $1/h_L$. Calculations show that this slope depends on the value of β_1 but is nearly independent of κ_1, see lines A, B and C, D in Fig. 16. For β_1 fixed, $\mathsf{L}(\beta_1, \kappa_1)$ is shifted horizontally by changing the value of κ_1. Thus, there is a one-to-one correspondence between couples (β_1, κ_1) $(\beta_1 > 0, \kappa_1 > 0)$ and straight lines $\mathsf{L}(\beta_1, \kappa_1)$ of positive slope in the log-log diagram of Fig. 16. The material parameters (β_1, κ_1) defining nonlocal plasticity can be uniquely defined from the best fit of $\mathsf{L}(\beta_1, \kappa_1)$ with experimental data.

From (66) and (69) it follows that, for given value of β_1 and of the stress amplitude σ^-, $\left|\dot{\varepsilon}^p\right|_{\max} \propto \kappa_1^{1/2\beta_1}$. Thus, for two different values κ_{1A} and κ_{1B} the magnitudes of plastic strain rate corresponding to a given σ^- are related by the following relationship,

$$\frac{\left|\dot{\varepsilon}_A^p\right|_{\max}}{\left|\dot{\varepsilon}_B^p\right|_{\max}} = \left(\frac{\kappa_{1A}}{\kappa_{1B}}\right)^{-1/2\beta_1} \tag{70}$$

Note that this quantity is not dependent on the stress amplitude σ^-.

Therefore, considering the lines A and B in Fig. 16, respectively, associated with ($\beta_1 = 1, \kappa_{1A} = 103$) and ($\beta_1 = 1, \kappa_{1B} = 412$), one has $\left|\dot{\varepsilon}_A^p\right|_{\max} = 2\left|\dot{\varepsilon}_B^p\right|_{\max}$ for any value of σ^-. Similarly, between lines C ($\beta_1 = 0.5, \kappa_{1C} = 7.5x10^5 N$) and D ($\beta_1 = 0.5, \kappa_{1D} = 15x10^5 N$) one has $\left|\dot{\varepsilon}_C^p\right|_{\max} = 2\left|\dot{\varepsilon}_D^p\right|_{\max}$.

For a given characteristic length L^* and stress Σ, consider the family of lines defined as,

$$\mathsf{F}(\mathrm{L}^*, \Sigma) = \left\{ \mathsf{L}(\beta_1, \kappa_1) \quad \text{such that} \quad \Sigma = \kappa_1 L^{*-2\beta_1} \right\} \tag{71}$$

It can be motivated from scaling arguments and verified numerically that all the lines of $\mathsf{F}(\mathrm{L}^*, \Sigma)$ have an unique intersection point. Let us denote by F_I and F_J the families with intersection points respectively I and J. Examples are shown in Fig. 16 of families F_I (F_J) with lines A and C converging at I (lines D and B converging at J). In the example shown in Fig. 16 the characteristic length associated to F_I has the value $\mathrm{L}_\mathrm{I}^* = 0.137$ mm and the value of L_J^* is double that of the above value (0.274 mm).

Consider in general the family F_J obtained by horizontal translation of F_I with magnitude defined by $\delta = \dot{\varepsilon}_I^p / \dot{\varepsilon}_J^p$, as illustrated in Fig. 16 for $\delta = 2$. Defining by $(\mathrm{L}_\mathrm{I}^*, \Sigma_I)$ ($(\mathrm{L}_\mathrm{JI}^*, \Sigma_J)$) the characteristic length and stress associated to F_I (F_J), it is proven in Appendix A that $L_J^* / L_I^* = \delta$ and $\Sigma_I = \Sigma_J$.

Similar considerations could be developed for the first gradient plasticity model (48). A one-to-one correspondence can also be found between the parameters (β , κ) defining non-local plasticity and straight lines with positive slope in the diagrams of Fig. 15 or Fig. 16.

Figure17 shows the variation of the stress amplitude σ^- in terms of the maximum of the plastic strain rate for the two laminates PC37/SS19 and PC74/SS37. Experimental results are well described by the second gradient plasticity model (60) with $\beta_1 = 0.5$ and $\kappa_1 = 7.5\text{x}10^5$ N

for PC37/SS19, and $\kappa_1 = 15\text{x}10^5$ N for PC74/SS37. As for the first gradient model, κ_1 is scaled by the cell size (the value of κ_1 is doubled for PC74/SS37).

Results obtained for the PC37/SS19 laminate are summarized in Table 5 for the two gradient plasticity theories, and different values of the structure parameters β and κ. It is shown in Fig. 18 (see also Table 5) that values of structure parameters can be chosen so as to provide almost identical results for the first gradient ($\beta = 0.88$, $\kappa = 3.55$ MPa) and the second gradient approaches ($\beta_1 = 0.5$, $\kappa_1 = 7.5\text{x}10^5$ N). Therefore, the relationship between stress amplitude and maximum plastic strain rate is enough to characterize the structure parameters for a given gradient plasticity approach but is not sufficient to discriminate between the two plasticity theories considered here. The shape of the shock front provides additional information allowing favoring one of the theories. The smooth transition towards state (-) shown in Fig. 13 for the first gradient theory seems to be in better agreement with experimental shock profiles, Zhuang (2002, 2003).

6) Summary and conclusions

First and second gradient plasticity theories were used to describe steady shock waves propagating through laminates in the direction perpendicular to layers. The aim of this investigation was to analyze and model experimental results obtained for two laminates made of the same constituents. The only difference being that the layer's widths in the laminate PC74/SS37 are doubled when compared to those of PC37/SS19. The maximum strain rate within the shock layer was measured to be twice smaller for PC74/SS37. Experimental results could be represented by the power law (57), $\left|\dot{\varepsilon}^p\right|_{\max} = B\left(\sigma^-\right)^{h_L}$ where $\left|\dot{\varepsilon}^p\right|_{\max}$ is the maximum plastic strain rate and σ^- is the stress amplitude. The exponent h_L has the same value for both laminates (close to 1.8) , however *B* is twice larger for PC37/SS19 in comparion to the value for PC74/SS37.

These experimental results could be well described by using the first gradient plasticity model (48). In this approach, structure parameters κ and β are introduced to account for the internal structure of the laminate (layer's thickness and material properties of constituents). Since the volume fractions of phases are identical for both laminates, the difference in the material response can be related to the laminate cell size, L. The present modeling shows that $\left|\dot{\varepsilon}^p\right|_{\max} \propto \frac{1}{L}$. The experimental finding that the strain rate within the shock layer is twice larger in PC37/SS19 than in PC74/SS37 is then rationalized.

Similar results were found by using the second order gradient plasticity approach (60). Experimental results are well described by taking a non-linear dependence of the flow stress with respect to the second gradient of plastic deformation, with exponent $\beta_1 = 0.5$ in (60).

Non-local effects are described in these gradient plasticity theories by two material parameters, β and κ. It was shown, that for a given plasticity theory, these parameters (β, κ) could be uniquely determined from experimental results. However, both plasticity theories provide results of comparable quality when compared to experimental data relating the stress amplitude to the maximum of the plastic strain rate. Nevertheless, the first gradient plasticity approach can be favored when comparing the shape of the shock front to experimental data.

Viscous effects, which have been neglected in the present modeling, have sometimes a major role in structuring shock fronts as for example in polycrystalline metals. In the latter case, experimental results show a power law dependence between the stress jump across the plastic shock and the maximum strain rate, with exponent h=4, Swegle and Grady (1985), a value much larger than those of h_L for laminates (of the order of 2).

The present theory can be augmented to account for viscous effects. However, the experiments performed on laminates indicate that the scaling of the shock layer is mostly related to the laminate internal structure (in particular to the cell size). Viscous effects, which, for metals and polymers, can be related to basic mechanisms of visco-plastic deformation, are not able to account for such scaling. Dispersion effects due to heterogeneities of the laminate structure are thought to be all the more important, as the contrast between the mechanical properties of constituents is larger. In the case of a large contrast, wave dispersion appears to be the dominant factor structuring the shock front and viscosity is believed to play a minor role.

Table 1: Material characteristics of polycarbonate and stainless steel

	Poisson ratio	Elastic shear modulus	Mass density
PC (Polycarbonate)	0.37	0.94 Gpa	1190 kg/m^3
SS (Stainless steel)	0.29	77 Gpa	7890 kg/m^3

Table 2: Overall material characteristics of the laminates PC37/SS19 and PC74/SS37

	c_{1111}	c_{1122}	b	ρ_0	S	c^+
PC37/SS19 and PC74/SS37	6.84 Gpa	3.60 Gpa	66.7	3468 kg/m^3	2.1	1600m/s

Table 3: Experimental data for the shock velocity C and the particle velocity v^-

PC37/SS19							
C (km/s)	1.96	1.89	2.39	2.32	2.33	2.53	3.12
v^-(km/s)	0.254	0.254	0.454	0.454	0.485	0.485	0.699
PC74/SS37							
C (km/s)	1.94	2.39					
v^-(km/s)	0.257	0.527					

Table 4: Parameters related to the laminate internal structure

	L_1	L_2	κ	
PC37/SS19	0.37 mm	0.19 mm	1.7	m.MPa
PC74/SS37	0.74 mm	0.37 mm	3.4	m.MPa

Table 5: Theoretical results for the PC37/SS19 laminate using the values of material parameters given in Table 2.

			First gradient κ=1.7 m MPa		Second gradient κ_1 =750 m^2 MPa	
$\sigma^-(GPa)$	$v^-(m/s)$	C(m/s)	$\left\|\dot{\varepsilon}^p\right\|_{\max}$ (s^{-1}x10^6)	w (mm)	$\left\|\dot{\varepsilon}^p\right\|_{\max}$ (s^{-1}x10^6)	w_1 (mm)
8	748	3084	6.15	0.117	3.93	0.183
6	615	2811	3.69	0.160	2.75	0.215
4	461	2497	1.79	0.246	1.64	0.268
2	273	2112	0.51	0.490	0.648	0.385

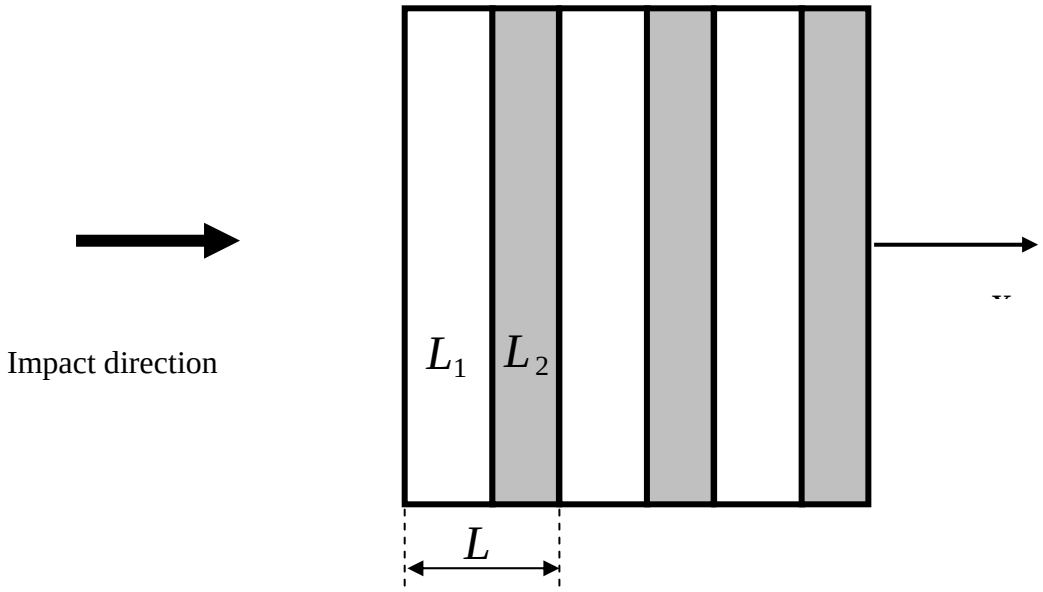

Fig.1: Schematic of the geometry of a periodically layered composite with layer's thicknesses L_1 and L_2

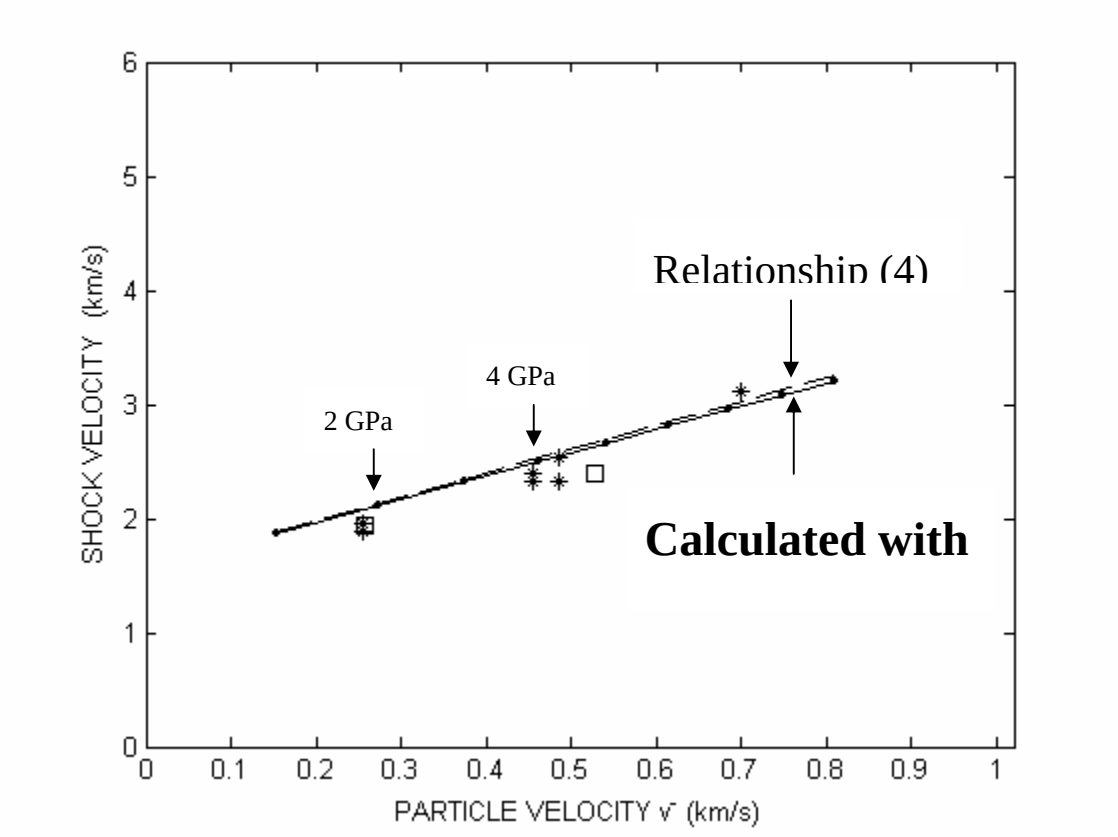

Fig.2: Shock velocity C versus particle velocity v^- at the rear of the plastic shock. Experimental data are represented by stars and squares respectively for PC37/SS19 and PC74//SS37 laminates. The dashed line is given by equ. (4) with slope $S=2.1$, $v^+=18.2m/s$ and $c^+=1600m/s$. The solid line with dots corresponds to calculations made in section 4.2 by using the Hugoniot defined by (39)

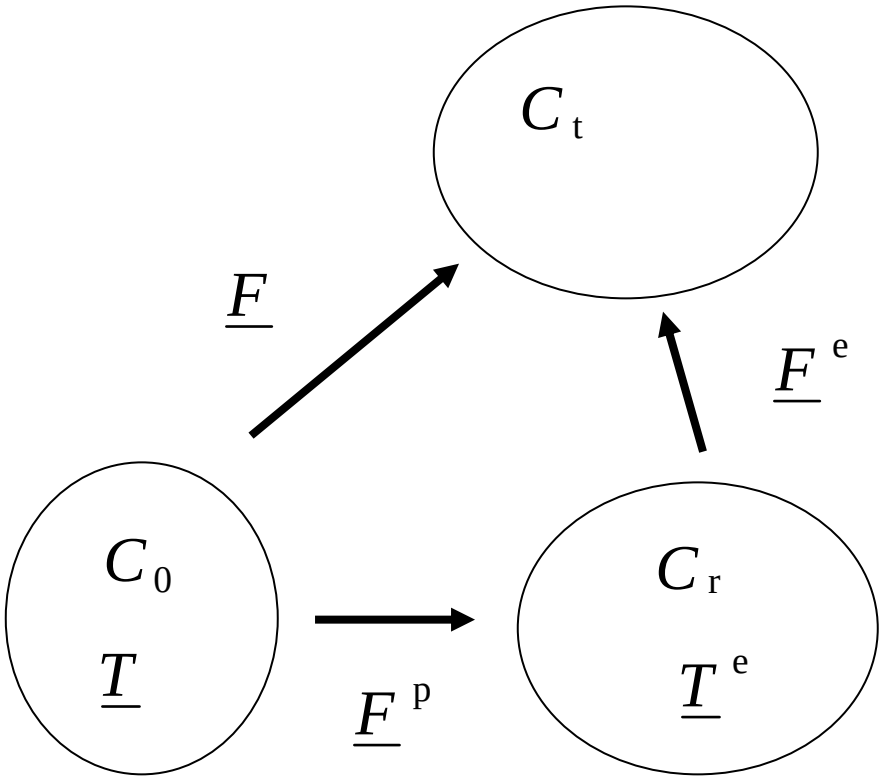

Fig.3: Decomposition of the deformation gradient $\underline{F}$ into plastic part $\underline{F}^p$ and elastic part $\underline{F}^e$.

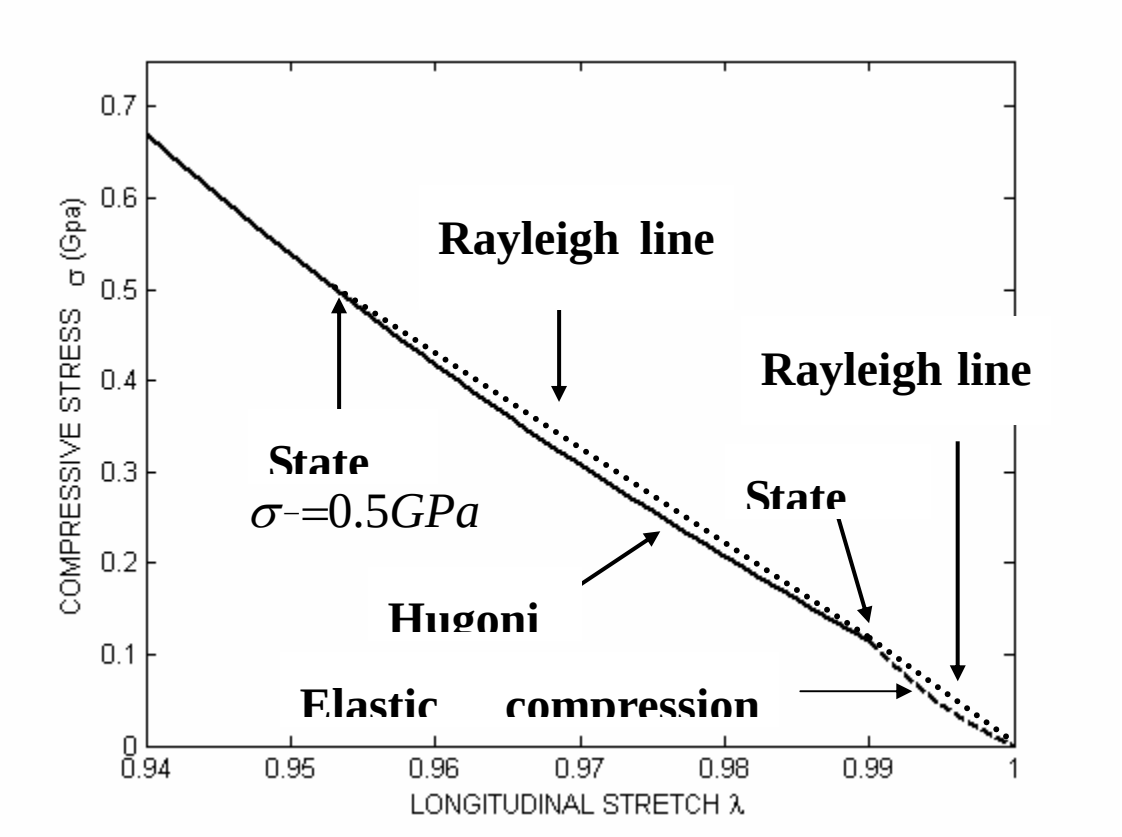

Fig.4: Plastic shock for the stress amplitude $\sigma^- = 0.5GPa$. The material is first compressed from the initial state to the state (+) by an elastic shock (elastic precursor), and is further compressed by a plastic shock from state (+) to state (-). These two distinct shocks exist if the condition (41) on shock velocities is satisfied.

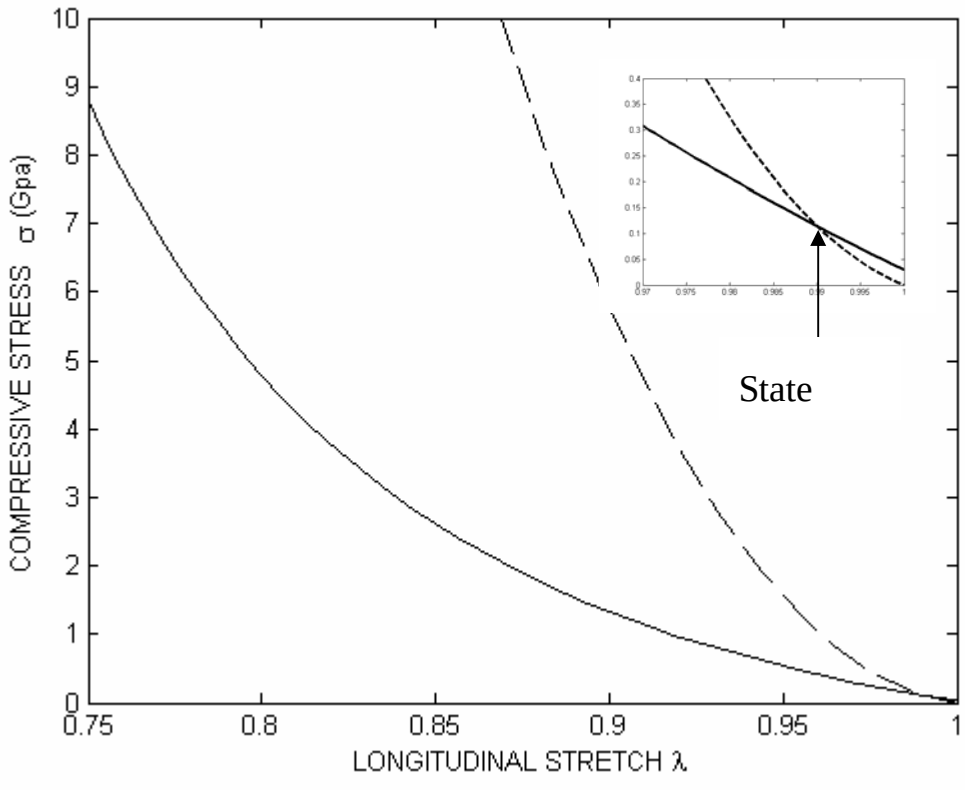

Fig.5: Hugoniot curve (solid line) and elastic loading path $\lambda \to \sigma = -T_{11}(\lambda, 1)$ (dashed line) for the laminate PC37/SS19. Results are identical for PC74/SS37. A zoom is shown for $0.97 \leq \lambda \leq 1$ in the upper part of the figure.

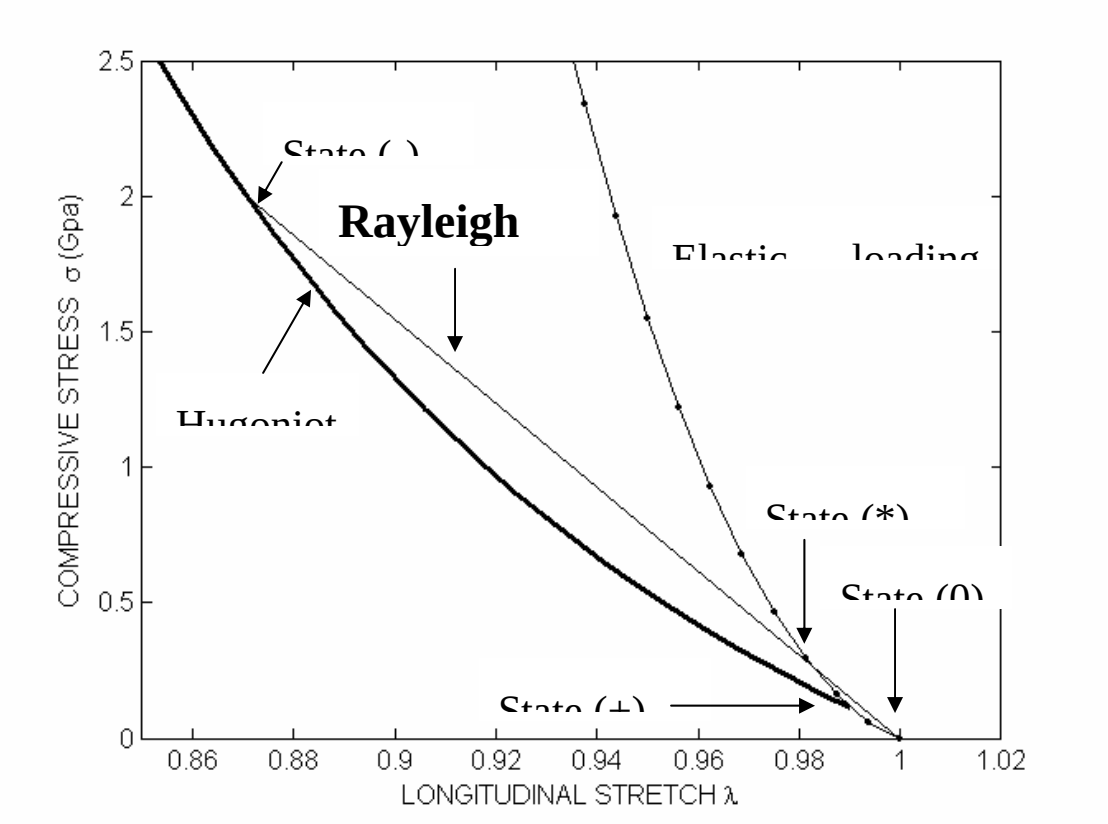

Fig.6: Elasto-plastic shock generated for a large enough stress amplitude such that condition (41) is not satisfied.

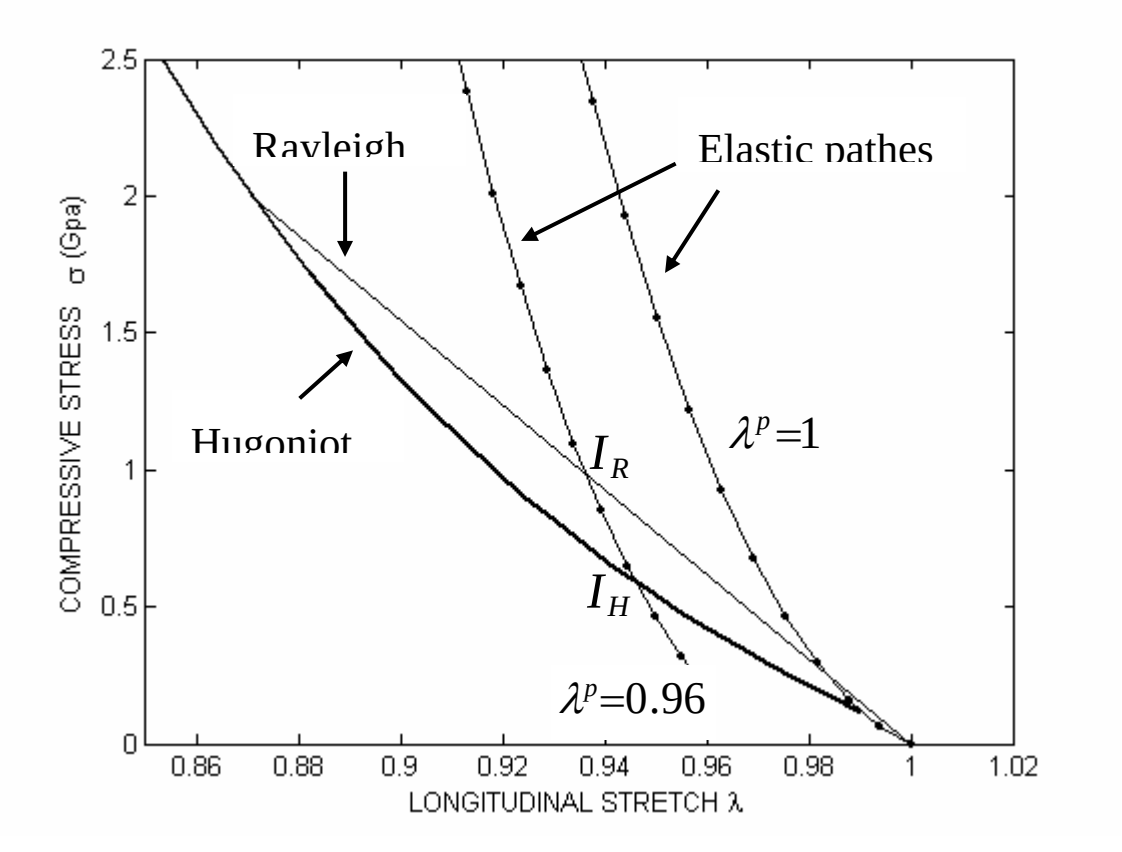

Fig.7: The elastic loading path corresponding to the fixed value of the plastic stretch $\lambda^p=0.96$ intercepts the Hugoniot at I_H and the Rayleigh line at I_R. The shock stress amplitude is $\sigma^-=2GPa$.

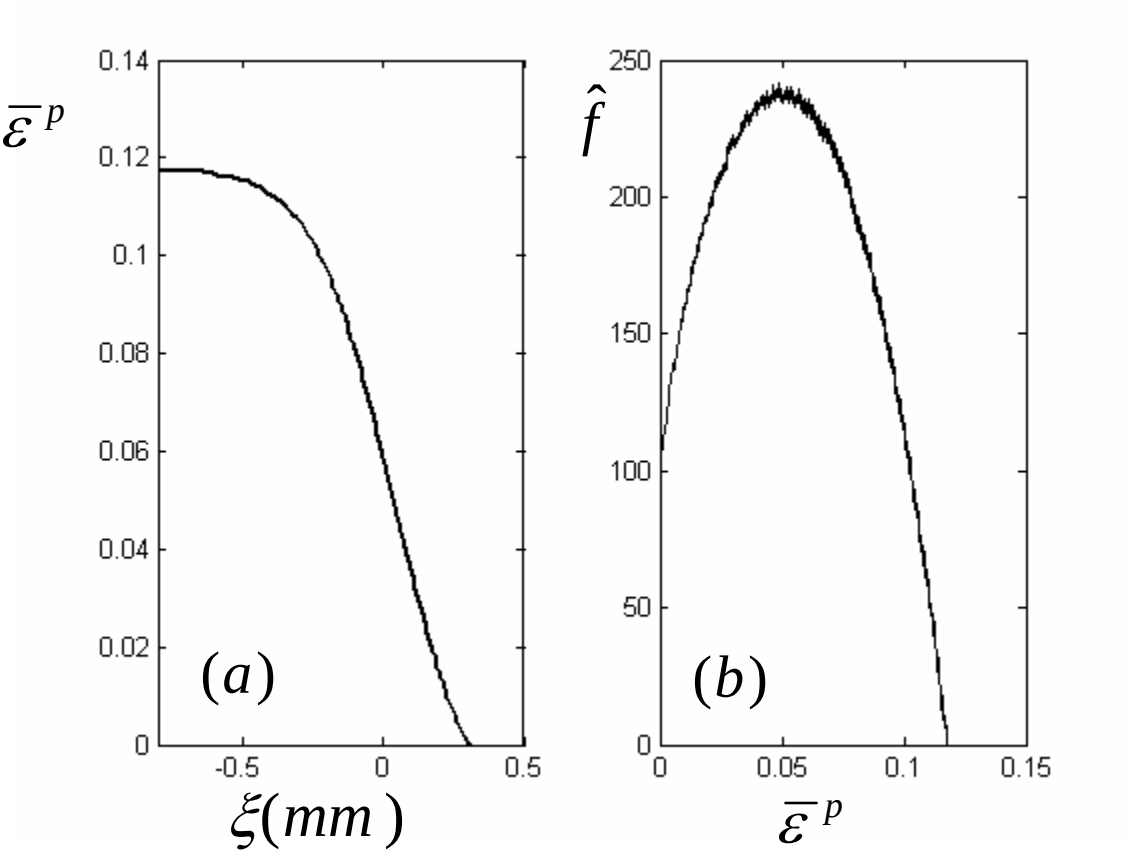

Fig.8: Structure of the plastic shock for $\sigma^- = 2GPa$:

(a) distribution of the cumulated plastic deformation $\overline{\varepsilon}^p$ in terms of the position ξ

(b) variation of the function $\hat{f}(\overline{\varepsilon}^p)$ defined by (52)

The first order gradient plasticity theory is used here with $\kappa = 1.7\ m\ Mpa$, $\beta = 1$.

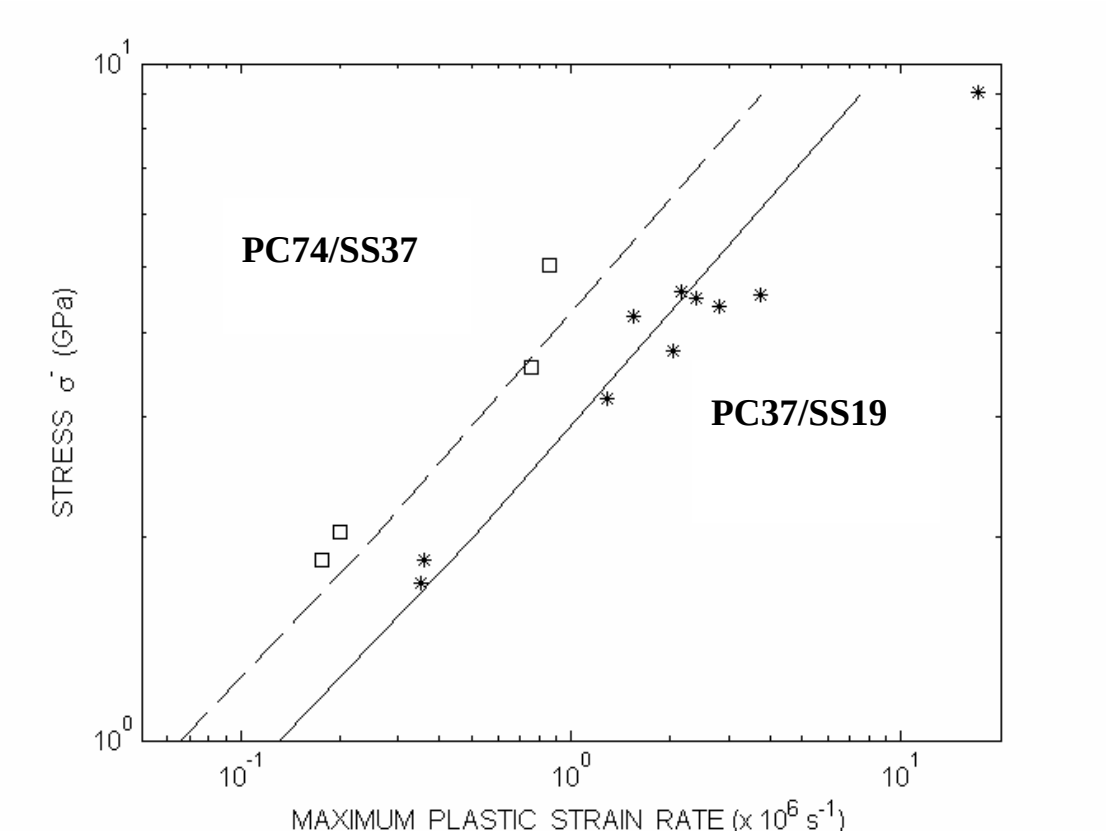

Fig.9: Stress amplitude σ^- in terms of the maximum of the plastic strain rate within the shock layer. Experimental results for the laminates PC37/SS19 and PC74/SS37 are respectively represented by stars and squares . Results of the first gradient modelling are obtained for $\beta = 1;\quad \kappa = 1.7\, m\, Mpa$ is used for PC37/SS19 and κ=3.4$m.MPa$ for PC74/SS37. Note that doubling the value of κ for PC74/SS37 is the direct consequence of the layer's thicknesses of PC74/SS37 being twice those of PC37/SS19.

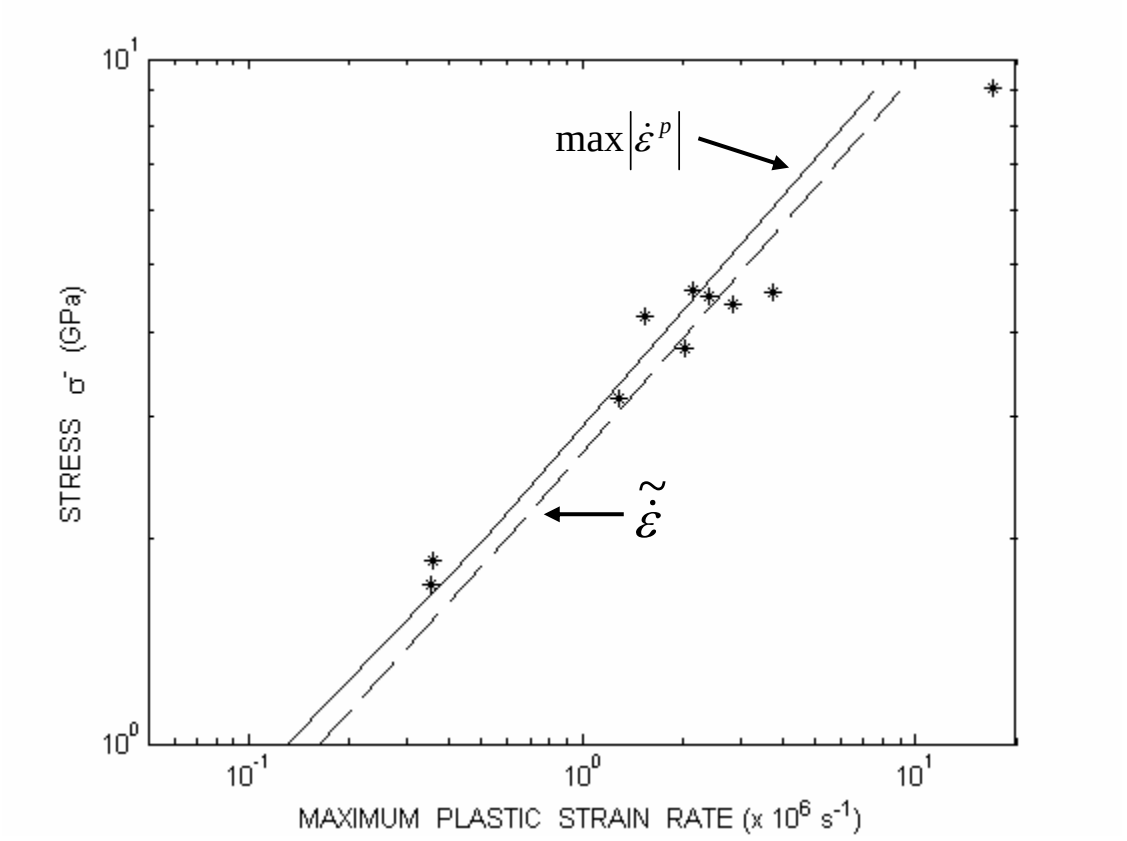

Fig10: Stress amplitude σ^- in terms respectively of :

- the maximum of the plastic strain rate $\left|\dot{\varepsilon}^p\right|_{\max}$ within the shock layer

- an estimate of the maximum of the strain rate within the shock layer $\tilde{\dot{\varepsilon}}$.

Stars represent experimental data for the laminates PC37/SS19. Results of the modelling are obtained for the first gradient theory with κ=1.7$m.MPa$ and $\beta = 1$.

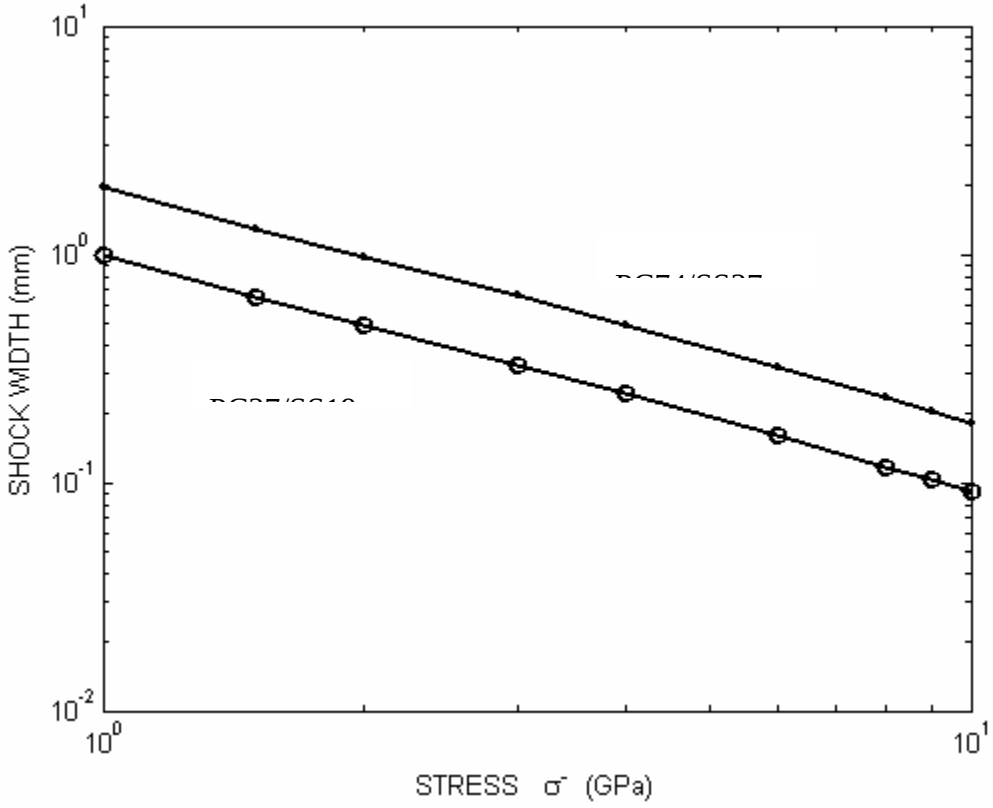

Fig.11: Shock width w estimated with (55). Note that the shock width for PC74/SS37 is twice that for PC37/SS19. Dots correspond to the following stress amplitudes (Gpa): 1, 1.5, 2, 3, 4, 6, 8, 9, 10.

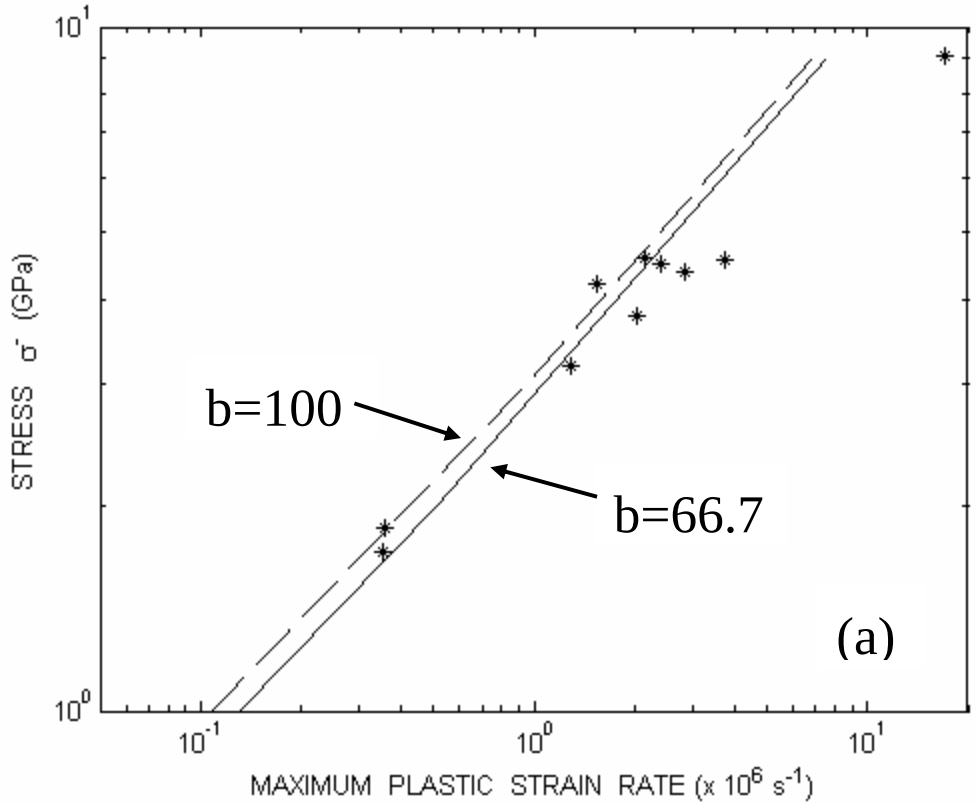
STRESS σ' (GPa)
MAXIMUM PLASTIC STRAIN RATE (x 10^6 s^-1)
b=100
b=66.7
(a)

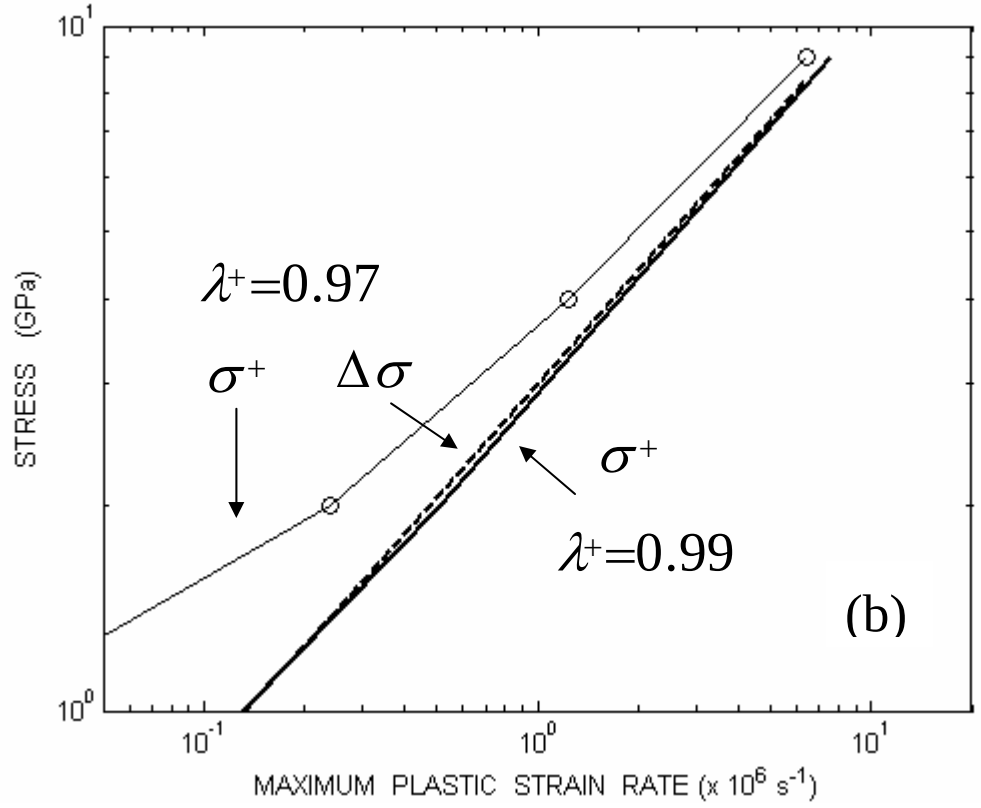

Fig.12: Effects of second order elastic constants (a) and of λ^+ (b)

(a) Stress amplitude σ^- in terms of the plastic strain rate $\left|\dot{\varepsilon}^p\right|_{\max}$ for two values of the parameter b which scales second order elastic constants. Results with b=100 are compared with the previous results of Fig.9 obtained with b=66.7. Stars are experimental data for the PC37/SS19 laminate.

(b) Effect of λ^+ (defining the state (+)). The solid line corresponds to the previous results of Fig.9 (σ^- versus $\left|\dot{\varepsilon}^p\right|_{\max}$ with $\lambda^+=0.99$). Two different curves are shown for $\lambda^+=0.97$. The solid line with dots represents σ^- in terms of $\left|\dot{\varepsilon}^p\right|_{\max}$ The dashed line shows the variation of the stress jump $\Delta\sigma=\sigma^--\sigma^+$ with respect to $\left|\dot{\varepsilon}^p\right|_{\max}$.

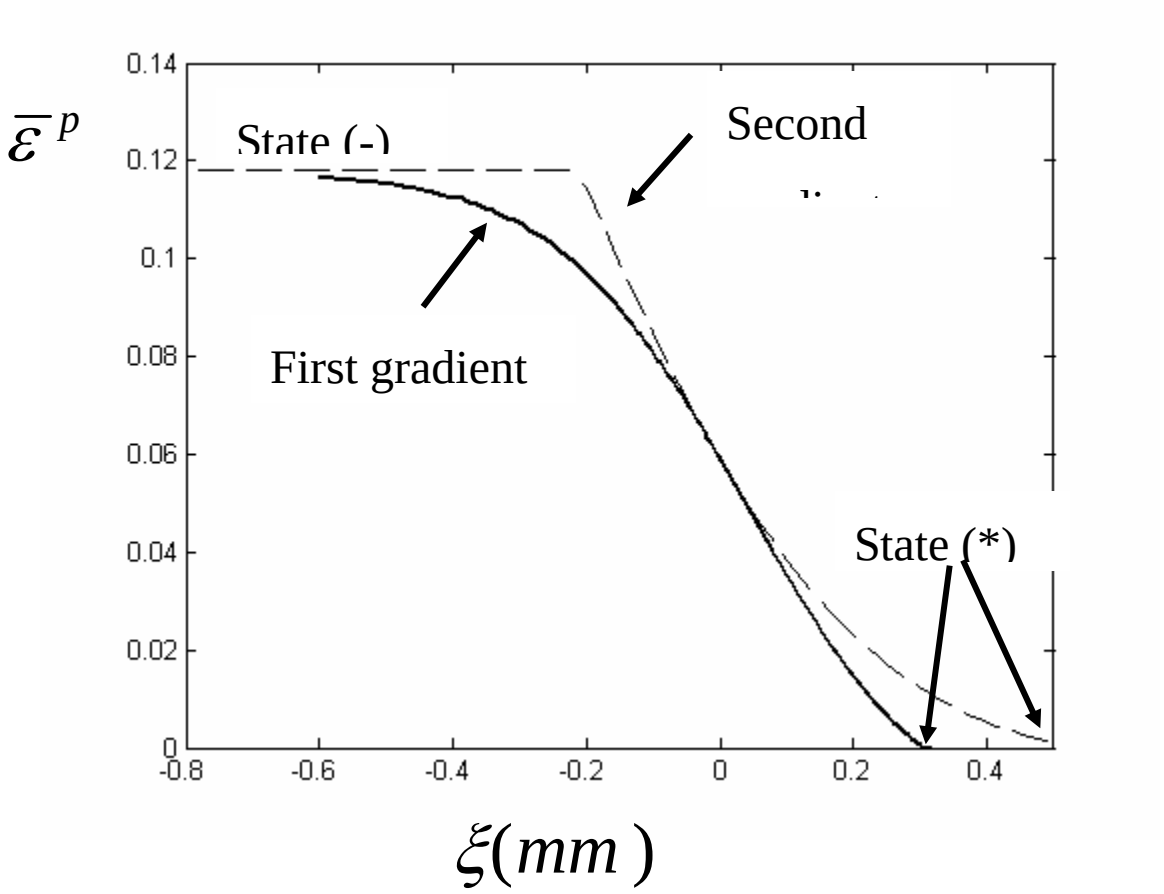

Fig.13: Distribution within the shock structure of the cumulated plastic deformation $\overline{\varepsilon}^{p}$ in terms of the position. The first gradient plasticity theory defined by (48) with ($\beta = 1$, κ=1.7$m.MPa$) is compared to the second gradient theory (60) with ($\beta_1 = 1, \kappa_1 = 750N$). The stress amplitude is $\sigma^{-} = 2GPa$.

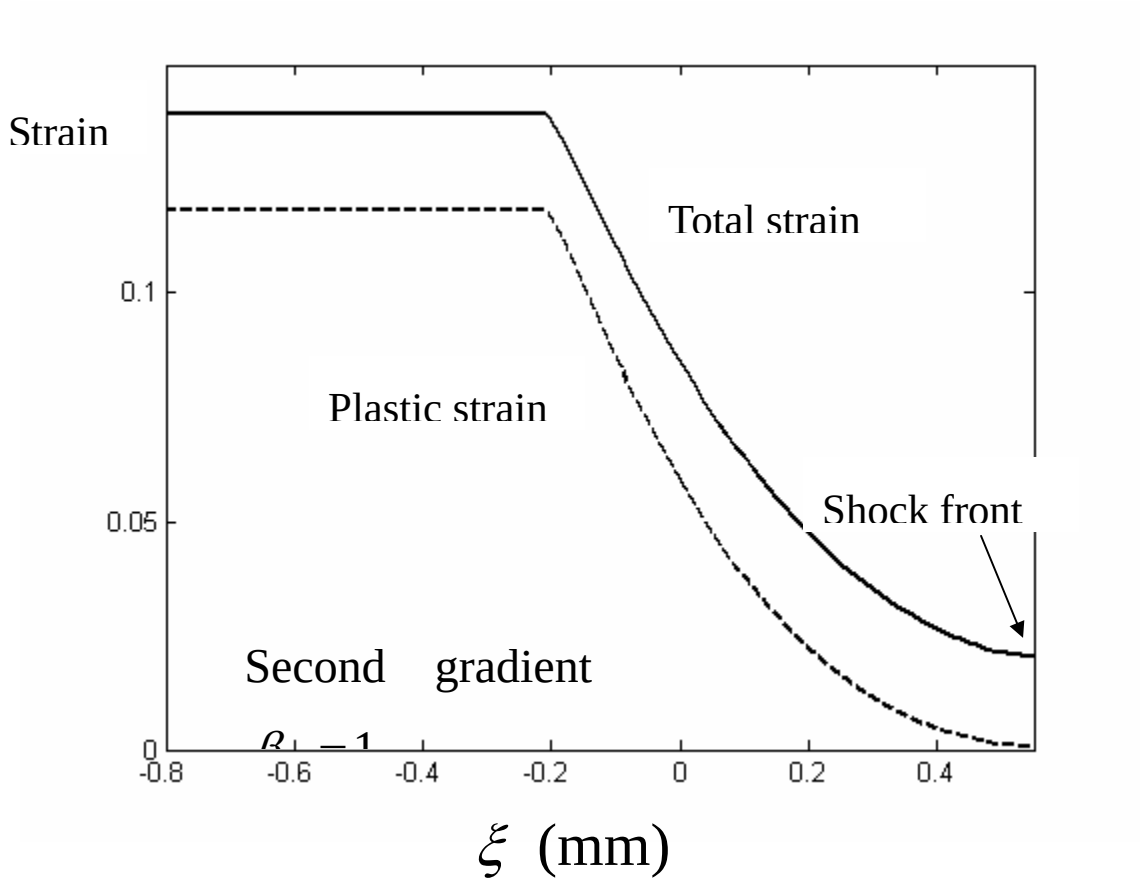

Fig.14: Shock wave profiles calculated for $\sigma^{-} = 2GPa$ with the second gradient approach ($\beta_1 = 1, \kappa_1 = 750N$). The dashed and the solid lines correspond respectively to distributions of the plastic strain $\bar{\varepsilon}^p$ and of the absolute value of the total strain $|\varepsilon| = |\log(\lambda)|$.

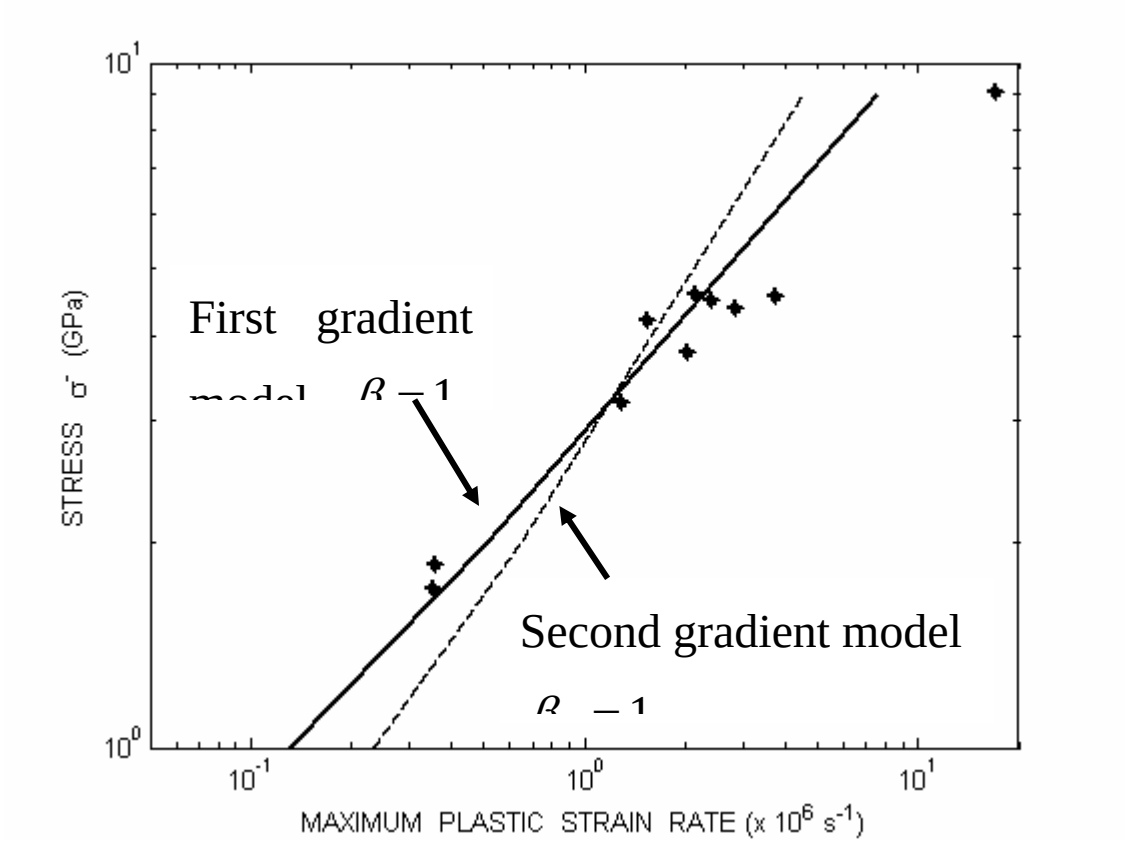

Fig.15: Compared to the first gradient model, the slope of the (dashed) line associated to the second gradient model (with $\beta_1 = 1$) is not adequate to account for experimental results of PC37/SS19 (stars)

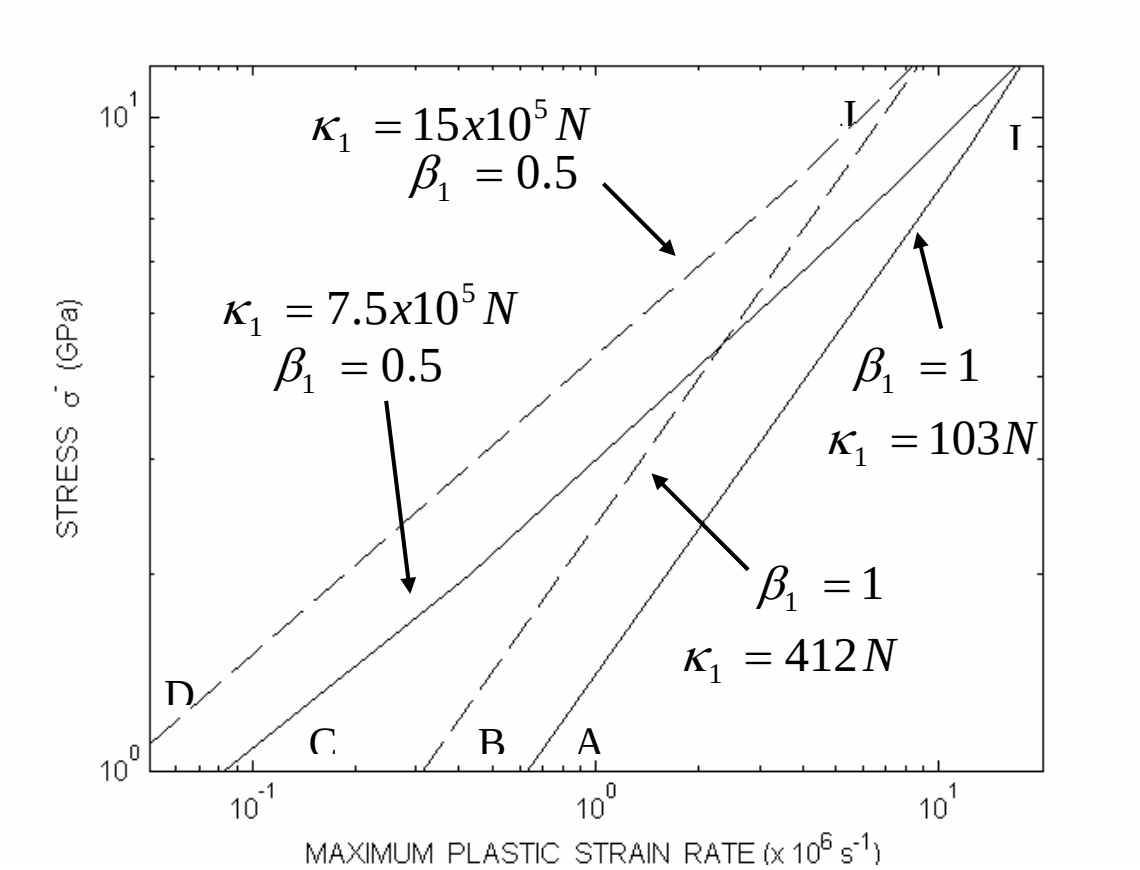

Fig.16: Second gradient approach: effects of parameters β_1 and κ_1 on the relationship between stress amplitude and magnitude of plastic strain rate. The slope depends on the value of β_1 but is not dependent upon κ_1. For a given value of β_1, the lines are shifted horizontally by changing the value of κ_1.

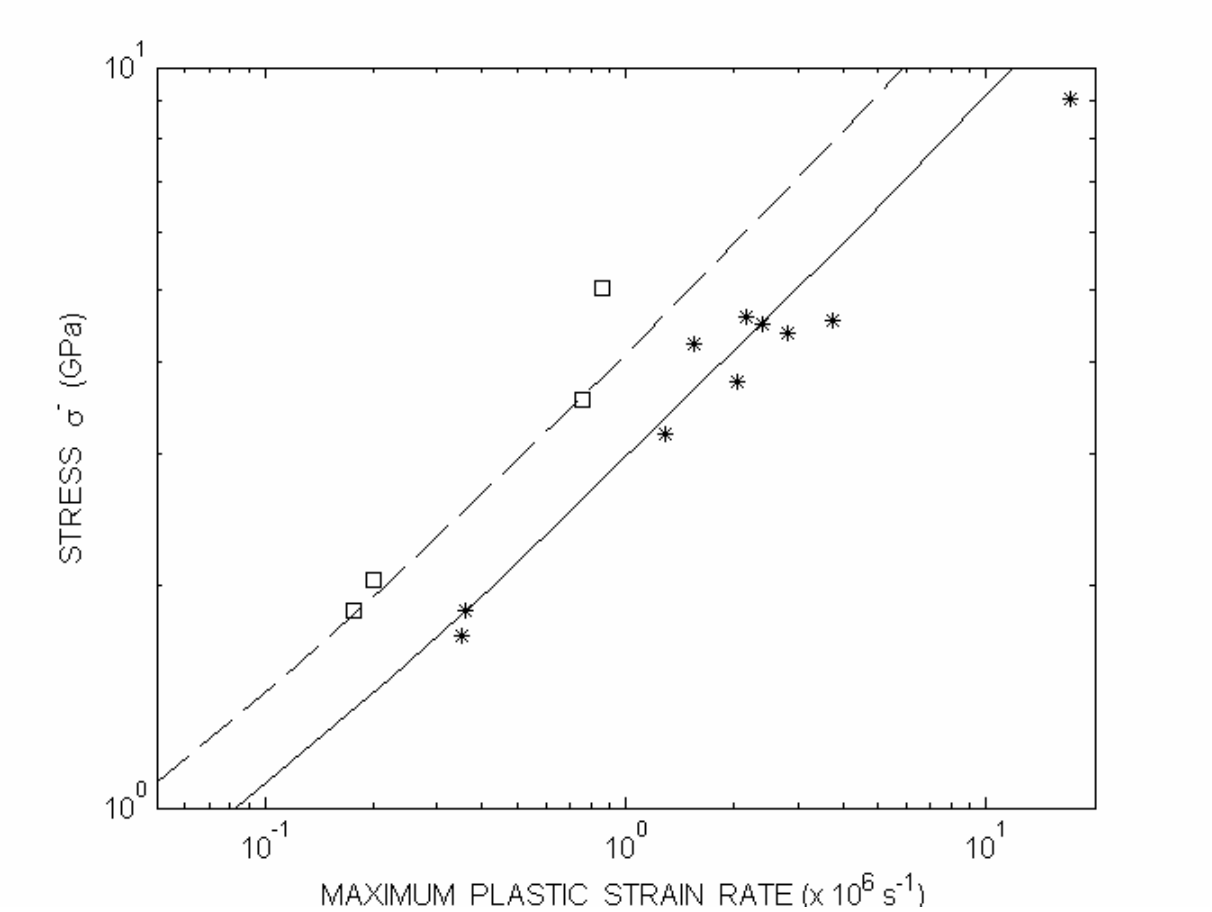

Fig.17 : Stress amplitude $\dot{\sigma}$ in terms of the maximum of the plastic strain rate within the shock layer. Experimental results for the laminates PC37/SS19 and PC74/SS37 are respectively represented by stars and squares. Results of the second gradient modelling (60) are obtained for $\beta_1 = 0.5$ and $\kappa_1 = 7.5x10^5 N$ (PC37/SS19), $\kappa_1 = 15x10^5 N$ (PC74/SS37). As for the first gradient model, κ_1 is scaled by the cell size which is multiplied by two for PC74/SS37.

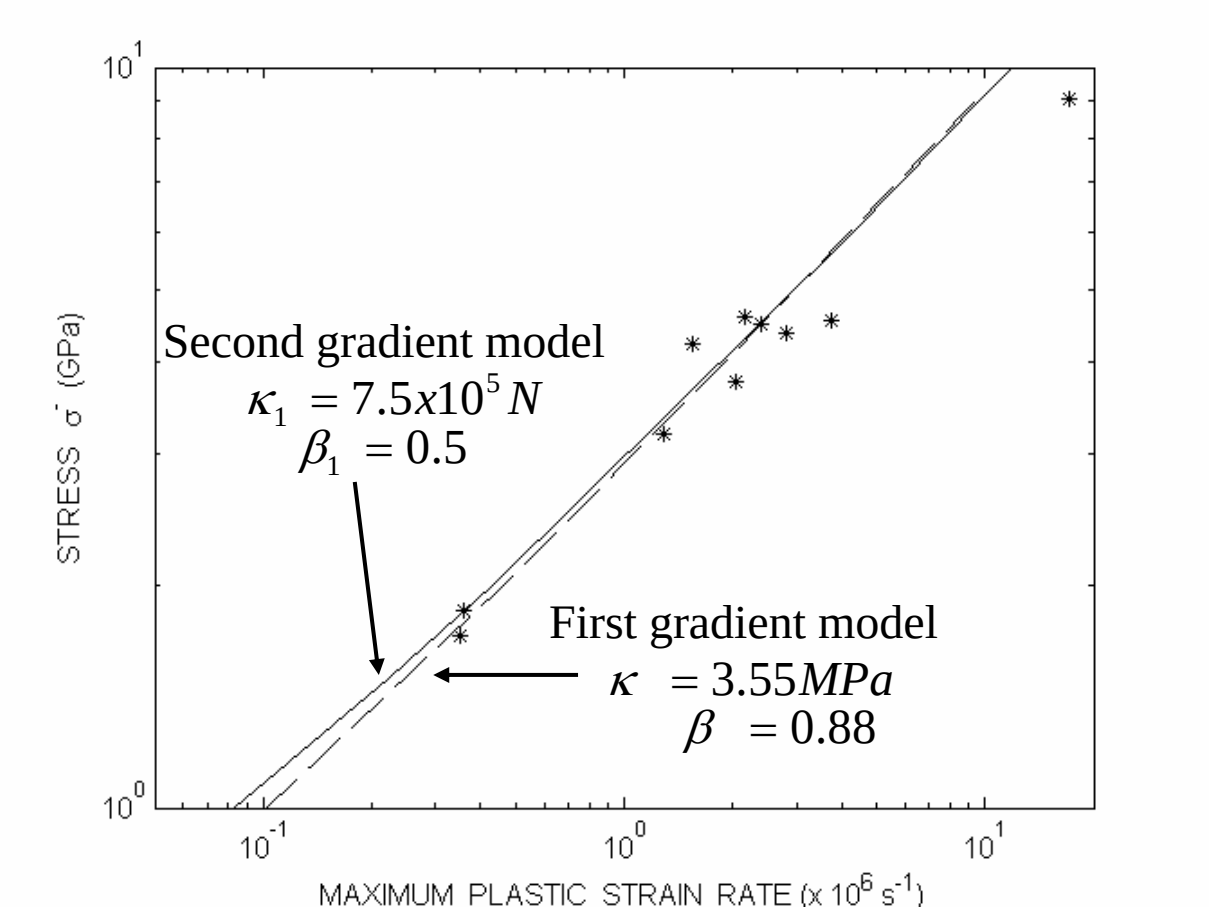

Fig.18 : First gradient approach ($\beta = 0.88$, $\kappa = 3.55$ MPa) compared to second gradient approach ($\beta_1 = 0.5$, $\kappa_1 = 7.5x10^5$ N), respectively dashed and solid lines. Stars represent experimental data for PC37/SS19.

References

Achenbach, J.D., "A Theory of Elasticity with Microstructure for Directionally Reinforced Composites," International Center for Mechanical Sciences, Courses No. 167, Springer, New York, 1973.

Aifantis, E.C., *Mech. Materials*, 35, 259-280, 2003.

Benson, D.J. and V.F. Nesterenko, "Anomalous decay of shock impulses in laminated composites", *J. Appl. Phys.*, 89, 3622-3626, 2001.

Boutin C., *Int J. Solids Structures*, 33, 1023-1051, 1996.

Chree C., *Q. J. Pure Appl. Math*, 23, 335, 1889.

Christensen, R.M., "Mechanics of Composite Materials," John Wiley and Sons, New York,1979

Clifton, R. J., "On the analysis of elastic/visco-plastic waves of finite uniaxial strain", in *Shock Waves and the Mechanical Properties of Solids*, J. J. Burke and V. Weiss, Eds., Syracuse University Press, 1971.

Eringen A.C., *Int. J. Engng. Sci.*, 10, 425-435, 1972.

Eringen A.C., "Nonlocal polar Field Theories," Continuum Physics, Vol. 4, A.C. Eringen, Ed., Academic Press, New York, 205-267, 1976.

Fleck, N.A. and J.W. Hutchinson, *J. Mech. Phys. Solids*, 41, 1825-1857, 1993.

Fleck, N.A. and J.W. Hutchinson, *J. Mech. Phys. Solids*, 49, 2245-2271, 2001.

Gao, H., Y. Huang, W.D. Nix and J.W. Hutchinson, *J. Mech. Phys. Solids*, 47, 1239-1263, 1999.

Grady, D., *J. Mech. Phys. Solids*, 46, 2017-2032, 1998.

Green A.E., and R.S. Rivlin, *Archives for Rational Mechanics and Analysis*, 17, 113-147 (1964)

Huang Y., H. Gao, W.D. Nix and J.W. Hutchinson, *J. Mech. Phys. Solids*, 48, 99-128, 2000.

Kunin, I.A., "Elastic Media with Microstructure," Vol. 1 and 2, Springer, Berlin, 1982 and 1983.

Lubarda, V. A., "Elastoplasticity Theory", CRC Press, Boca Raton, Florida 2001.

Luciano, R. and J.R. Willis, "Non-local response of a random laminate subjected to configuration body force," *J. Mech. Phys. Solids, ,* 49, 431-444, 2001.

Lundergan, C.D. and D.S. Drumheller "Dispersion of shock waves in composite materials," in *Shock Waves and the Mechanical Properties of Solids*, J. J. Burke and V. Weiss, Eds., Syracuse University Press, 1971.

Mindlin, R.D., "Micro-structure in linear elasticity," *Arch. Rational Mech. Analysis*, 16, 51-78, 1964.

Molinari, A. and G. Ravichandran, *J. Appl. Phys*., 95, 1718-1732 , 2004.

Nesterenko, V.F., Formin V.M. and P.A. Cheskidov, "Attenuation of strong shock waves in

laminate materials", in "Nonlinear deformation waves" (Edited by U. Nigul and J. Engelbrecht), Springer-Verlag, Berlin, 191-197, 1983.

Nesterenko, V.F., "Dynamics of heterogeneous materials," Springer-Verlag, New-York, 2001.

Pochhammer L., *J. Reine Angew. Math*, 81, 324, 1876.

Rice, M. H., R. G. McQueen and J. M. Walsh, "Compression of Solids by Strong Shock Waves", in *Solid State Physics*, F. Seitz and D. Turnbull, Eds., 1958.

Sun, C.T., J.D. Achenbach and G. Hermann, *J. Appl. Mech.*, 35, 468-475, 1968.

Swegle, J. W. and D. E. Grady, *J. Appl. Phys*., 58, 692-701, 1985.

Whitham, G.B., "Linear and Nonlinear Waves", J. Wiley, New York, 1974.

Zhuang, S., "Shock wave propagation in periodically layered composites," Ph.D. Thesis, California Institute of Technology, 2002.

Zhuang, S., G. Ravichandran and D.E. Grady, *J. Mech. Phys. Solids*, 51, 245-265, 2003.

Appendix A

The family $\mathsf{F}(L_I^*, \Sigma_I)$ of lines intersecting at point I, is translated horizontally as shown in Fig. 16 into the family $\mathsf{F}(L_J^*, \Sigma_J)$ of lines intersecting at point J. Considering in $\mathsf{F}(L_I^*, \Sigma_I)$ the lines $\mathsf{L}(\beta_{1A}, \kappa_{1A})$ and $\mathsf{L}(\beta_{1C}, \kappa_{1C})$, denoted for simplicity as *A* and *C*, one obtains, from (71),

$$\Sigma_I = \kappa_{1A} L_I^{*-2\beta_{1A}} = \kappa_{1C} L_I^{*-2\beta_{1C}} . \qquad \text{(A1)}$$

The lines *B* and *D* are obtained by horizontal translation of *A* and *C* and intersect at *J*, therefore they are in $\mathsf{F}(L_J^*, \Sigma_J)$ and from (71),

$$\Sigma_J = \kappa_{1B} L_J^{*-2\beta_{1A}} = \kappa_{1D} L_I^{*-2\beta_{1C}} \qquad \text{(A2)}$$

where the following relationship has been used,

$$\beta_{1A} = \beta_{1B} , \qquad \beta_{1C} = \beta_{1D} . \qquad \text{(A3)}$$

The magnitude of the translation $\mathsf{F}(L_I^*, \Sigma_I) \rightarrow \mathsf{F}(L_J^*, \Sigma_J)$ is characterized by the ratio $a = \dot{\varepsilon}_I^p / \dot{\varepsilon}_J^p$. Since lines *A* and *C* intersect at *I* and *B* and *D* intersect at J, for any stress amplitude σ^- one obtains,

$$\frac{\left|\dot{\varepsilon}_A^p\right|_{\max}}{\left|\dot{\varepsilon}_B^p\right|_{\max}} = \frac{\left|\dot{\varepsilon}_C^p\right|_{\max}}{\left|\dot{\varepsilon}_D^p\right|_{\max}} = a \tag{A4}$$

From (70), it follows that,

$$\left(\frac{\kappa_{1A}}{\kappa_{1B}}\right)^{-1/2\beta_{1A}} = \left(\frac{\kappa_{1C}}{\kappa_{1D}}\right)^{-1/2\beta_{1C}} = a \tag{A5}$$

and from (A1) and (A2),

$$L_I^* = \left(\frac{\kappa_{1A}}{\kappa_{1C}}\right)^{\frac{1}{2(\beta_{1A}-\beta_{1C})}} \quad , \qquad L_j^* = \left(\frac{\kappa_{1B}}{\kappa_{1D}}\right)^{\frac{1}{2(\beta_{1A}-\beta_{1C})}} \tag{A6}$$

Combining (A5) and (A6), it is found that,

$$L_J^* = aL_I^* \tag{A7}$$

and from (A1) and (A2),

$$\frac{\Sigma_I}{\Sigma_J} = \frac{\kappa_{1A}}{\kappa_{1B}}\left(\frac{L_J^*}{L_I^*}\right)^{2\beta_{1A}} = 1\,. \tag{A8}$$